COMPUTATIONAL MODELING OF NEUROMUSCULAR CONTROL OF VOLUNTARY SINGLE JOINT MOVEMENT

By

ALEX KRASNER

A thesis submitted to the

Graduate School-New Brunswick

Rutgers, The State University of New Jersey

in partial fulfillment of the requirements

for the degree of

Master of SCIENCE

Graduate Program in BIOMEDICAL ENGINEERING

written under the direction of

DR. WILLIAM CRAELIUS

and approved by

_____

_____

_____

_____

New Brunswick, New Jersey

[May 2014]

ABSTRACT OF THE THESIS

COMPUTATIONAL MODELING OF NEUROMUSCULAR CONTROL OF VOLUNTARY SINGLE JOINT MOVEMENT

by ALEX KRASNER

Thesis Director:

Dr. William Craelius

While the neuromuscular components involved in moving human joints are well known, there is no unifying model describing how they accomplish it. The dynamics of each individual neuromuscular component, from the brain structures, including cerebral cortex and sub-cortical areas, to the spinal cord, to the contractual apparatus have been formulated previously, but they have not been thoroughly tested, nor integrated into a holistic model of movement. This thesis combined these formulations into a single brain-spinal cord-muscle (BSM) model that illustrates motion planning by interactions between these brain components .

Movement plans originating in the cerebral cortex are processed in the descending motor pathways: brainstem, cerebellum, and spinal circuitry. Execution is coordinated by activation of agonist and antagonist muscle groups, mostly with closed-loop feedback control.

Here, I analyzed previously published neuromuscular formulations by simulations. I applied several methods for combining piecemeal models of individual components into a unified control system. Results with BSM produced physiologically

realistic joint outputs showing new details, not seen in previous models. The BSM model can be useful for detailed analysis of any biological component involved with motion generation, and can help in understanding the underlying causes of motor impairments.

Acknowledgments

I would like to sincerely thank Dr. William Craelius for his guidance, support, and patience during my graduate studies at Rutgers University. With his help, I was able to explore the boundaries of biomedical engineering and formulate my own ideas. I am grateful to have been under his mentorship.

I would also like to thank Dr. Daniel Bullock and Dr. Stephen Grossberg from Boston University, and Dr. Paul Cisek from the University of Montreal, with whom I held correspondence. Their guidance and advice were indispensable for the completion of this thesis.

Additionally, I am grateful for the help and motivation from my lab members: Maria Qadri, Qi Li, Dr. Nam H. Kim, and Dr. Nicki Newby; as well as the guidance from previous lab members. My experiences at the Rutgers Biomechanics and Rehabilitation Engineering Laboratory are responsible for my understanding of biomedical engineering and research.

Table of Contents

Abstract....ii
Acknowledgements....iv
List of Illustrations:....vii
Abbreviations:.... x
Introduction:.... 1
Hypotheses:.... 2
Literature Review: 3
I. Muscle models 3
i. Extrafusal fibers.... 3
ii. Riener and Quintern(RQ) model of muscle 5
iii. Intrafusal fibers 9
iv. Mileusnic et al. model 10
v. Golgi Tendon Organ.... 13
vi.VA model 13
vii. α-γ Co-activation and β Motoneurons.... 15
viii. Discussion 15
II. Joint model 16
i. Single joint model.... 17
ii. Multi-joint model 19
iii. Discussion 20
III. Involuntary CNS 20
i. VITE-FLETE-CBM (Part 1) 23
ii. Cerebellum 29
iii. VITE-FLETE-CBM (Part 2).... 30
iv. VITE-FLETE-CBM Results.... 32
v. CMAC 32
vi. Cortical VITE.... 33
IV. Voluntary CNS.... 37
i. Basal Ganglia.... 38
ii. Prefrontal Cortex.... 39
iii. Parietal Cortex.... 40
iv. Premotor Cortex and Supplementary Motor Area.... 41
v. Basal ganglia - thalamocortical model 42
vi. Adaptive Resonance Theory.... 46
vii. TELOS model.... 50
viii. LIST PARSE.... 55
ix. lisTELOS.... 58
Simulation Results and Discussion:.... 60
I. VITE-FLETE-CBM.... 60

II. Cortical VITE model 63
III. Combined update VITE and FLETE-CBM model 66
IV. Contreras-Vidal & Stelmach (CVS) Basal Ganglia Model 70
V. LIST PARSE 71
VI. lisTELOS modified 73
Conclusions: 79
Bibliography: 84

List of Illustrations

Figure 1: Actin-myosin contractile force generation caused by the power stroke interaction. [1] .. 3
Figure 2:Dynamic motor unit model. Top: f(t) - stimulation frequency. j(t) - recruited muscle fibers from static recruitment model. fit(t) - fatigue scaling factor. Bottom: example impulse train response of this model. [5] 7
Figure 3: Hill model of an intrafusal fiber. Sensory zone models the non-contractile, bag region of the fiber. Polar zone models the contractile regions of the fiber, which are innervated by gamma motoneurons. [7] 11
Figure 4: Virtual Arm model consisting of a virtual muscle, muscle spindle, GTO models and the SIMM joint model. This model is open loop since predetermined α and γ motoneuron signal are required to drive it. [11] 14
Figure 5: Ankle joint elastic torque at various flexion angles, and a two different knee flexions (φ_k). Passive joint torque is depended on distal and proximal joint conditions. [15] 17
Figure 6: Single joint model relating an input muscle stimulation pattern to the produced joint motion. This model consists of the muscle activation stage that models isometric force generation, muscle contraction stage that models force - length and force - velocity properties of a contracting muscle fiber, and a segmental dynamics stage that models passive joint properties and effects of external forces. [16] 18
Figure 7: Joint coupling phase plots. Larger correlation between joint velocities indicates a higher degree of joint inter-dependency. [18] 20
Figure 8: Diagram of the cortico-spinal tract. The lateral CST decussates in the brainstem, while the anterior CST decussates in the mid-thoracic region of the spine. [22] 21
Figure 9: VITE-FLETE-CBM diagram. VITE subunit models the generation of motor commands by the primary motor cortex. FLETE models the function of the brainstem (red nucleus) and spinal interneurons. FLETE also models generation of motoneuron signals, afferent signals, and muscle contraction dynamics. CBM models the learning function of the cerebellum in response to motor errors. [23] 23
Figure 10: Basic laminar structure of the cerebellum. Mossy fibers bring afferent signals to the cerebellum, which capture motor error. Inferior olivary nucleus cells teach Purkinje cells the expected motor commands. In response to motor errors, Purkinje cells modify outgoing motor commands to reduce those errors [27] 29
Figure 11: Top: Cerebellar learning causes adaptation of weights between parallel fibers and Purkinje cells. Bottom: after multiple trials, motor errors are consolidated causing produced joint movement to better match the desired joint trajectory. [23] 32
Figure 12: Expanded VITE model that simulates the activities of tonic and phasic cells located in the primary motor cortex (area 4) and the posterior parietal cortex (area 5). OPV represents the generation of the efferent copy that is compared to afferent signals, prior to the computation of the perceived position vector. [32] 35
Figure 13: Diagram of the interactions between the cortex, basal ganglia, and thalamus. Green - dopamine stream, which can be excitatory or inhibitory. Red - excitatory glutamate steam. Blue - inhibitory GABA stream. [37] 38

Figure 14: Balancing effect of serotonin on the direct and indirect pathways of the basal ganglia. Cortical modulation of the DRN, affects the activity of D1 and D2 pathways in the striatum. [53] 44
Figure 15: Two layer ART network. The recognition layer contains previously experienced hypotheses. The most relevant hypothesis is relayed into the comparison layer via feedback weights to generate a prototype pattern. If the input pattern matches the prototype vector, the relevant hypothesis is strengthened via feed forward weights. If there is a mismatch, the input pattern generates a new hypothesis that can later be discarded or strengthened. The orienting subsystem monitors whether the input pattern is "close enough" to the prototype vector via a vigilance parameter. [54,56] 46
Figure 16: TELOS model. FEF generates saccade plans based on the visual stimuli. Plans compete in the nigro-thalamic basal ganglia. The winning plan is compared to the input pattern generated within the PPC. If the saccade plan agrees with the input pattern in the PPC, the nigro-collicular basal ganglia disinhibits the superior colliculus, thus producing a saccade burst. [58]. 51
Figure 17: Winning saccade plan from the FEF and the input pattern in the PPC must agree prior to saccade generation. If no plans are present and one saccade target exists, a reactive saccade will be produced. A detailed explanation of the panels in provided in the text. [58] 53
Figure 18: LIST PARSE model that describes the generation of motion to a stored target in working memory. [59] 55
Figure 19: lisTELOS model. This model contains the same features seen in the TELOS model, and working memory properties seen in the LIST PARSE model. [61]..... 58
Figure 20: VITE-FLETE-CBM simulink model. Two of each model is present to represent agonist and antagonist muscle control. Alpha motoneuron, static gamma motoneuron and dynamic motoneuron activity is monitored by Mi, Si, and Di, respectively. Agonist and antagonist muscles flex the joint. Afferents monitor muscle length and stretch velocities. 61
Figure 22: Acceleration-velocity phase plot of the joint trajectory in Figure 21. It is not ellipsoidal, and has large deformities caused by inaccuracies of the VITE-FLETE-CBM model. 62
Figure 21: Joint flexion trajectory for an intact model. 62
Figure 23: Oscillatory joint trajectory of an impaired model. Removing cerebellar control of alpha motoneurons, dis-inhibits their activity thus leading to instabilities in motion. 63
Figure 24: Cortical VITE simulink model. Although the VITE model is improved, the muscle fiber models and the spinal models are greatly simplified..... 64
Figure 25: Detailed view of the VITE model. Note the large cross-connectivity between agonist and antagonist control streams. This coordinates activation of these muscle groups. 65
Figure 26: Combined model with the expanded VITE model with the FLETE and CBM models. 67
Figure 27: Two intact trajectories generated by the combined model. Note the reduced overshoot compared to the original VITE-FLETE-CBM model. Note scale difference 69
Figure 29: Simulated Go signal generated by basal ganglia. Again, at the end of motion, this signal does not return to zero. 70
Figure 28: Agonist and antagonist alpha motoneuron signals. At the end of motion, these signals do not return to rest. 70

Figure 30: Thalamic gating signal generated by Contreras-Vidal's and Stelmach's model. At the end of motion, the Go signal returns to zero. 71
Figure 31: Activation levels of stored items in working memory. Although, their absolute activations may change, order of items is preserved. 72
Figure 32: Target position vector signals generated by the LIST PARSE model. At the end of motion, these signals return to zero, unlike the step function signals used in the VITE-FLETE-CBM model. 73
Figure 33: Target position vector signals generated for four consecutive targets. For the first second, the system remains at rest and is shown 4 targets in order. Next, the system recalls these targets from memory and produces TPVs for each discrete motion. 76
Figure 34: Top: Difference vector is used to determine the end of a motion and the recall of the next target. Bottom: Produced perceived position vectors. Note that the scale of these trajectories are not absolute. In both top and bottom: The purple trace is analogous to the superior colliculus burst due to the fixation point. 77
Figure 35: Scalar TPV represents the desired limb positions in space. Note that the fixation point TPV seen in figure 33 is no longer present since the movement distance is zero. Scalar TPV a serialized representation of TPV, representing both spatial and temporal information. 78

Abbreviations:

BSM – Brain - Spinal cord - Muscle Model

PWM – pulse width modulation

GTO – golgi tendon organ

CNS – central nervous system

VM – virtual muscle

VA – virtual arm

SIMM – Software for Interactive Musculoskeletal Modeling

DOF – degrees of freedom

MSMS –Musculo Skeletal Modeling Software

CST – corticospinal tract

RST – reticulospinal tract

M1 – primary motor cortex

VITE – vector-integration-to-endpoint

FLETE – Factorization of Length and Tension

CBM – cerebellum

NIP – nucleus interpositus cells

RN – red nucleus

TPV – target position vector

DV – difference vector

PPV – perceived position vector

OPV – outflow position vector

DVV – desired velocity vector

BG – basal ganglia

STN – subthalamic nucleus

GPi/e – globus pallidus internal/external

SNc –substantia nigra pars compacta

PFC – prefrontal cortex

SMA – supplementary motor area

PMC – premotor cortex

PPC – posterior parietal cortex

LIP – lateral intraparietal sulcus

MIP – medial intraparietal sulcus

ART – adaptive resonance theory

WTA – winner takes all

FEF – frontal eye fields

SC – superior colliculus

SEF – selection eye fields

Introduction:

Treatment of motor disabilities, such as spasticity and muscular sclerosis, is challenging due to poor understanding of their origins. Many studies have shown the effects of these debilitating diseases and have even proposed treatments to them, but results have not been significant [1]. Besides, the lack of understanding, there is often large differences in test results that attempt to quantify the severity of these diseases. Specifically, treatments that are directed at improving motor control, cannot be well managed due to lack of reliable metrics of motor function. Most clinically accepted metrics, such as the Ashworth scale, Modified Ashworth scale, and the Tardieu scale, are subjective: they rely on a resistance-to-passive motion assessment made by the physician [2]. Therefore, these metrics are open to large variability, thus limiting their utility in monitoring dosage of medicines. As a result, the medical establishment has called for new metrics [1].

Current metrics are based on passive motions. This means that a physician or a robot is required to exert external force onto a patient's limb, while assessing their resistance to motion. Usually this resistance is caused by increased muscle tone, ligament and tendon tone, as well as involuntary reflexes to motion. These are calculated, usually, based on the simple harmonic equation. An example of such test is the Wartenberg test, where the lower leg is elevated to a certain height and then let go to oscillate to rest [3]. Recordings of the angular trajectory of the leg is used to calculate stiffness and dampness of motion.

Although these methods may be effective in extracting certain limited parameters of a patient's motor function they are not useful in understand in the cause of these

problems. In a previous study, Krasner et al., proposed the use of active motion to gauge impairment severity. Instead of an external source moving a patient's limb, the patient himself was required to move their limb, at a comfortable pace, from one target to the next. For patients that still retain some ability to move, voluntary motion can provide insight into the causes of their impairment.

Control of voluntary motion is a complex process that involves many areas of the brain, spine, and muscles. Understanding of the causes of certain motion disorders can be achieved by creating a physiologically relevant motion model that includes these systems. Motion impairments can then be simulated by varying parameters of target systems to match recorded motion trajectories and physiological signals from patients. This method would provide a way to create personalized and targeted assessments of disability in individual patients, thus improving the outcome of treatments.

The goal of this thesis is to unify several previous models, each of which explains some component of movement control, so that a fuller picture of the 'chain of commands' from cortex to muscle, can be seen. I show how the various components interact to produce a realistic single joint trajectory. No attempts were made to quantify motoneuron outputs, since this is beyond the scope of the work.

Hypotheses:

1. A brain-spinal cord-muscle (BSM) model can simulate efferent and afferent control of joints, in both open and closed loop modes.
2. The BSM can reasonably replicate movements associated with certain brain disorders

3. Brain structures associated with eye saccade generation are functionally analogous to those associated with limb motion control.

Literature Review:

I. Muscle models

i. Extrafusal fibers

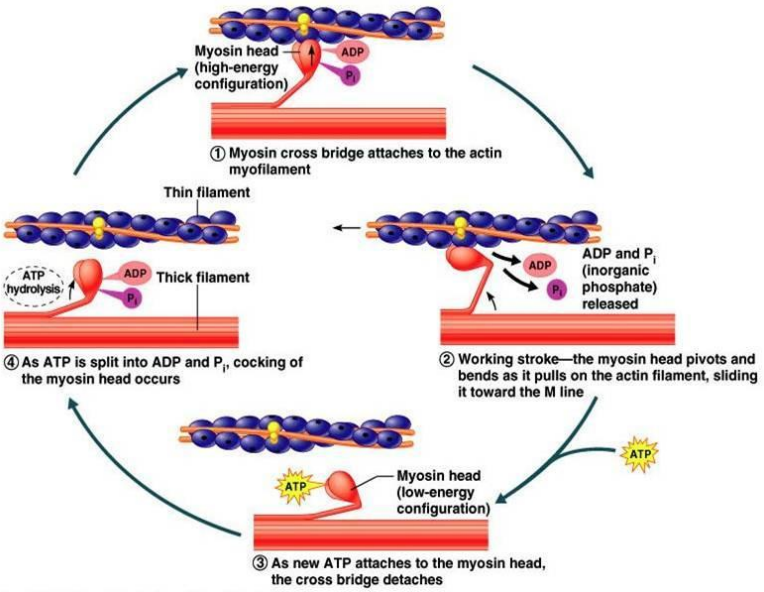

Figure 1: Actin-myosin contractile force generation caused by the power stroke interaction. [1]

Skeletal muscle consists of extrafusal and intrafusal fibers innervated by motoneurons. Extrafusal fibers are the force producing, contractile fibers that are innervated by alpha motoneurons. The most basic mechanism of their function is explained by the sliding - filament mechanism. This mechanism describes the interaction between actin and myosin filaments in the smallest contraction unit - the sarcomere [4].Figure 1shows the mechanism of a power stroke that causes contraction of the sarcomere. The power stroke initiates once the myosin heads bind to sites on . However, these actin binding sites are blocked by the tropomyosin protein at rest. Binding of $Ca^{2+}$to the troponin protein, located in proximity of tropomyosin, induces a conformational change of the tropomyosin protein, revealing the actin binding sites [4].

Thus, to model force generation by actin - myosin sliding, Ca^{2+} dynamics need to be modeled as well.

Long stretches of parallel sarcomere units are packed into myofibrils surrounded by, calcium ion containing, sarcoplasmic reticulum, which itself is surrounded by a transverse tubule network, also known as T-tubules [4,5]. T-tubules extend outwards to the sarcolemma. This whole encapsulated structure is known as the muscle fiber that can be innervated by only one motoneuron (while one motoneuron can innervate one or many muscle fibers).An action potential from the motoneuron causes the release of Acetylcholine (Ach) neurotransmitter into the neuromuscular junction that then causes the depolarization of the sarcolemma [4]. This process opens voltage gated Na^{+} channels, thereby propagating an action potential down the T-tubules and releasing Ca^{2+} from the sarcoplasmic reticulum.

Three different types of muscle fibers are present in skeletal muscle: slow - oxidative, fast - oxidative -glycolytic, and fast - glycolytic fibers, all differing in the contractile force they can produce and the duration that force can be sustained [4,5]. Depending on the force required for the task, these fiber types will be sequentially recruited to aid in force generation. The progression of increasing the number of muscle fibers is known as recruitment and proceeds in the order listed above. Slow - oxidative fibers are known as slow fibers or type I fibers and are characterized by having slow actin - myosin head binding rates, thus being able to produce moderate force, but for a prolonged period of time. Fast - oxidative - glycolytic and fast - glycolytic fibers are known as fast fibers or type II fibers and are characterized by having fast actin - myosin

head binding rates, thus being able to produce large contractile forces, but for a short time period [4].

The limited duration of force generation is known as fatigue, and is caused, in part, by a large release of Ca^{2+} ions from the sarcoplasmic reticulum [5]. When no free Ca^{2+} is present, more actin binding sites cannot be revealed, thus negating the contractile function of the muscle fiber.

ii. Riener and Quintern(RQ) model of muscle

The properties discussed above describe the physiology of extrafusal muscle fibers. Riener and Quintern developed a mathematical model of skeletal muscle force generation ability based on those properties [5]. It is a multi-compartmental model that features calcium dynamics, force generation via action - myosin power stroke, and fiber recruitment.

The model consists of two major subunits, one representing static recruitment of muscle fibers and the other the dynamic force generation by each motor unit. A lumped, innervating action potential from all motoneurons is simulated as a pulse - width modulated (PWM) signal. The pulse width and amplitude encode the number of recruited muscle fibers, and the signal frequency encodes the action potential itself, that will ultimately produce a contractile force [5].

In the RQ model, motor unit recruitment is modeled as a function of the pulse width of the incoming signal. If the pulse width exceeds the minimal threshold values then a muscle fiber is recruited. The amount of recruited fibers depends on how large the pulse width is compared to threshold. Greater pulse width results in a larger percentage of

recruited fibers. This model differentiates betweentype I and type II fibers [5]. These differ in threshold pulse width and maximal pulse width values. Amplitude of the PWM signal is not necessary, in fact, amplitude and pulse width can be used to encode for the same muscle recruitment. In their model, the PWM signal is assumed constant amplitude. Equation 1 describes the details of muscle fiber recruitment:

$$p_{rec}(d) = k_1\{(d - d_{thr})\arctan[k_{thr}(d - d_{thr})] - (d - d_{sat})\arctan[k_{sat}(d - d_{sat})]\} + k_2 \quad (1)$$

$$\ddot{\beta}(t) + c_1\dot{\beta}(t) + c_2\beta(t) = c_3\alpha(t) \quad (2)$$

$$\ddot{\gamma}(t) + c_4\dot{\gamma}(t) + c_5\gamma(t) = c_6\beta(t) \quad (3)$$

$$\dot{fit}(t) = \frac{1}{T_{fat}} * [fit_{min} - fit(t)] * \bar{\gamma}(t) + \frac{1}{T_{rec}} * [1 - fit(t)] * [1 - \bar{\gamma}(t)] \quad (4)$$

$$a(t) = \frac{a_0 + [\rho\gamma(t)fit(t)]^2}{1 + [\rho\gamma(t)fit(t)]^2} \quad (5)$$

$$\dot{F_i}(t) = \frac{1}{T_g} * [a(t) - F_i(t)] \quad (6)$$

Once a muscle fiber is recruited, its generated force is simulated by the dynamic motor unit model and is related to the frequency of stimulation. The model consists of six major submodels where each simulates a biological component of the muscle. The first submodel is the impulse generator which simulates action potentials from the motoneuron. Action potentials are represented as 1ms half sine waves repeating at the stimulation frequency rate - α(t). These action potentials are inputted into the T - tubule model. This model accounts for the depolarization of the T -tubule membrane and is modeled by a second order over damped transfer function, shown in Equation 2. Depolarization of the T - tubules causes a release of Ca^{2+} from the sarcoplasmic reticulum. This release is modeled as an over damped second order system in the 3rd subsystem (see Equation 3). This concentration can be modified if the muscle fiber is

fatigued. Fatigue is modeled as a first order transfer function that depends on the current state of the fiber and the normalized amount of calcium ion to be released, $\bar{\gamma}(t)$. Two time constants are associated with the rate of fatigue and recovery over Ca^{2+}; these are T_{fat} and T_{rec}, respectively. Equation 4 describes the fatigue constant that modulates the amount of Ca^{2+} released for the sarcoplasmic reticulum. The authors name this value as the muscle fitness value. The 5thsubmodel simulates calcium ion binding as a non-linear function of Ca^{2+} concentration (Equation 5). Finally, generated muscle force is estimated by a gliding model which simulates myosin-action power stroke (Equation 6). Total contractile force is the sum of the forces produced by slow and fast motor units. Figure 2illustrates the described dynamic motor unit model.

For validation of the model, three paraplegic subjects were tested [5]. Quadriceps were innervated with surface electrodes and the moment at the knee was measured. Since the leg was fixed the generated moment is proportional to the isometric muscle force. Parameter for the model were determined by trial and error to maximize the simulated output to a training output.

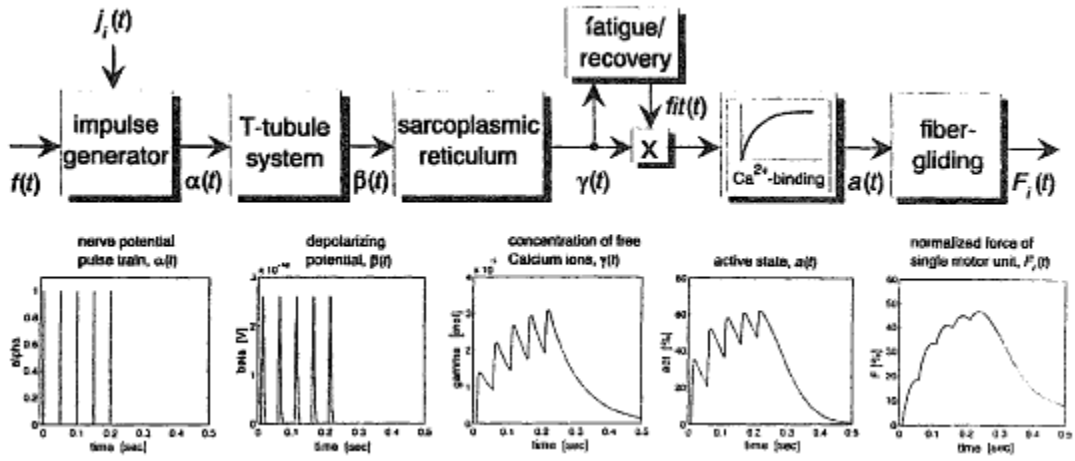

Figure 2:Dynamic motor unit model. Top: f(t) - stimulation frequency. j(t) - recruited muscle fibers from static recruitment model. fit(t) - fatigue scaling factor. Bottom: example impulse train response of this model. [5]

The RQ model makes many assumption and omissions that, for modeling voluntary motion, can be important. The contractile force predicted by this model relates only to the maximal isometric force that the muscle can produce. However, flexion and extension are not isometric tasks; they are, more often, isotonic tasks. Thus it would be important to consider the force - length relationship property of muscle contraction, and the force - velocity property [6]. These properties are caused by actin - myosin binding abilities at various contraction lengths and velocities, and by the structural composition of muscle fibers.

Passive force- length relationship is caused by the presence of connective tissue that surrounds each muscle fiber [6]. Increasing the length of the muscle far beyond its resting length causes an increasing amount of restorative, contractile, force. This is caused by the elastic property of connective tissue. Active force - length relationship is caused by the amount of actin - myosin overlap present in each sarcomere. Maximal contraction force is generated generally within 30% change of the resting length (0.7Lo - 1.3Lo) [4,6]. Beyond these ranges the amount of generated force decreases.

Force - velocity relationship relates to the shortening velocity of a muscle fiber when an external load is present. An isometric task, for example, has just enough load to prevent the muscle fiber from reducing length, even when force is being generated. When the load is light, a muscle fiber will shorten at a certain rate that depends on the load. The lighter the load, the fast the fiber will contract. This is known as concentric contraction. When loads are heavy, the muscle may still try to exert force, but will be stretched by the load, thus extending and not shortening. The heavier the load, the fast the fiber will extend. This is known as eccentric contraction.

Both of these properties, concentric and eccentric contraction, need to be modeled, or implied in the model, to predict voluntary motion.

iii. Intrafusal fibers

Besides extrafusal fibers, muscles are also composed of intrafusal fibers are run in parallel. These fibers are responsible for monitoring velocity, length and tension of extrafusal muscle fibers and reporting them back to the central nervous system (CNS). All intrafusal fibers are bundled into one structure known as the muscle spindle and encapsulated by connective tissue.

Intrafusal fibers are innervated by dynamic or static gamma motoneurons depending on the type of fiber. Signals from gamma motoneurons modulate the response of intrafusal fibers. Fibers send afferent signals back to the CNS via three types of neurons: Ia - responsible for monitoring stretch velocity, II - responsible for monitoring muscle length, and Ib, which isn't located in the muscle spindle, but is responsible for monitoring muscle tension.

Muscle spindles contain three types of intrafusal fibers: nuclear bag_1 fibers, nuclear bag_2 fibers and nuclear chain fibers [7,8]. These differ in their monitoring function and the type of gamma motoneuron they respond to. Nuclear bag fibers are specialized muscle fibers with all the nuclei gathered in the central region, known as the "bag". The bag region is not contractile, and is more compliant than the contractile peripheral regions [8]. This allows the nuclear bag fiber to be sensitive to stretch and stretch velocity. The afferent fiber is wound around the bag region and thus acts like a mechanoreceptor. The peripheral regions of the nuclear bag fiber can be innervated by a gamma motoneuron, thus they can contract in response to feedback signals.$Bag_1$and bag_2

fibers differ mainly in size and function. Bag_2 fibers are larger and sensitive to length, while bag_1 fibers are thinner and are sensitive to stretch velocity [8]. Nuclear chain fibers do not have a bag region with aggregated nuclei, and are less compliant than nuclear bag fibers [8]. These fibers monitor muscle length.

Usually there is only one nuclear bag_1fiber in the muscle spindle. It is innervated by the dynamic gamma motoneuron that modulates its sensitivity to changes in stretch velocity [8]. By contracting the peripheral regions of the intrafusal fiber, dynamic gamma motoneuron signals adjust for slack in the nuclear bag_1 fiber caused by rapid flexion or extension. Ultimately, the process of readjusting the nuclear bag fiber, modulates the response of the Ia afferent by accommodating for muscle length changes due to contraction.

Muscle spindles also contain 1 - 4 nuclear bag_2 fibers and at least twice as many nuclear chain fibers that are both innervated by static gamma motoneurons. Static gamma neurons modulate the sensitivity of these fibers. However, unlike for bag_1 fibers and Ia afferents, the static gamma motoneuron affects the sensitivity to length change in these fibers. The response of the II afferent is the sum of responses of the bag_2 fibers and the chain fibers [7,8].

Despite the differences in the three types of intrafusal fibers, discussed above, most studies view the muscle spindle as a single entity with a lumped Ia afferent, responsible for monitoring stretch velocity, and a lumped II afferent, responsible for monitoring stretch length.

iv. Mileusnic et al. model

A study by Mileusnic presented a detailed model of muscle spindle function [7]. This model did differentiate between the different intrafusal fiber types, and is therefore one of the most detailed model to date.

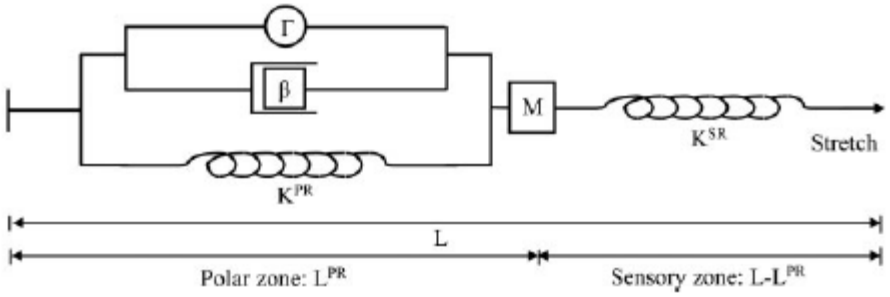

Figure 3: Hill model of an intrafusal fiber. Sensory zone models the non-contractile, bag region of the fiber. Polar zone models the contractile regions of the fiber, which are innervated by gamma motoneurons. [7]

This study modeled the intrafusal fibers as a complex spring - dashpot model, shown in Figure 3, resembling the Hill muscle model. One of these models was used to model nuclear bag_1 fibers, and another modeled nuclear bag_2 and nuclear chain fibers as a lumped unit [7]. The spring - dashpot model used contains both a polar region, analogous to the contractile peripheral regions of an intrafusal fiber, and a sensory region, analogous the non contractile bag region. The polar zone contains a contractile element, Γ, which is innervated by the dynamic or static motoneuron. The contractile force generated by this unit is a linear function of fusimotor activity, f, which is a related to the firing frequency of each gamma motoneuron [7]. Mileunsnic modeled the fusimotor activity using the biochemical Hill equation for both the dynamic and static motoneurons [7]. An example of the dynamic fusimotor activity is shown in Equation 7.

$$\frac{df_{dyn}}{dt} = \frac{\frac{\gamma_{dyn}^2}{\gamma_{dyn}^2 + 60^2} - f_{dyn}}{\tau} \tag{7}$$

Where τ represents an activation time constant and γ_{dyn} represents the activity of the (dynamic) gamma motoneuron.

Fusimotor activity was introduced into the model to relate actual, real world, gamma motoneuron firing rates, to the activation levels of the polar regions of the intrafusal fibers. Fusimotor activities scale the maximal contractile force of the polar region from zero (no contraction/activation) to maximal.

A similar concept was used to relate the stretch of the sensory region to the firing rate of the Ia or II afferents. The stretch of the sensory and polar regions in the different intrafusal fibers was scaled by a constant, G, to obtain real - world estimates of afferent firing rates.Ia afferent was determined to receive a nonlinearly summed signal from bag_1, bag_2 and chain files, while II afferent was determined to receive a summed signal from bag_2 and chain fibers [7]. Neuro-physiological studies have shown that Ia afferents, indeed, take inputs from both nuclear bag fibers, and chain fibers, although majority of the signal is received from the bag fibers.

The model was able to match experimental data that recorded Ia and II afferent firing rates when a muscle spindle was stretched under various conditions. The fiber was extended +/- 10% of its optimal resting length, either in a ramp or triangular pattern [7]. Afferent signals were recorded in the presence and absence of gamma motoneuron activation.

Although the model predicted afferent firing rates very closely, the test was performed in relatively tight conditions, as stated before. It is difficult to assess the validity of this model at fiber lengths much larger or smaller than the optimal resting

length. However, this model is the best muscle spindle model, since it improves upon many previous models.

v. Golgi Tendon Organ

As noted, the Ib afferent monitors the muscle during motion and provides feedback to the CNS. The Ib afferent is not located in the muscle spindle, but rather in the Golgi tendon organ (GTO). These afferents monitor muscle fiber tension and may protect the muscle from excessive loads as they may cause the muscle to tear. The GTO is an encapsulated collagen structure that is located between the muscle and tendon [8]. Since it is arranged in series with the muscle, rather than in parallel like muscle spindles, the GTO can respond to tensile force. Increases in force cause the collagen fibers in the GTO structure to become taut, which pinches the Ib afferent. Thereby a signal related to the applied stretch force is relayed to the CNS.Mileusnic created another spring-dashpot model to replicate the function of the GTO under different loading conditions [9]. Based on his model results , the Ib firing rate is approximately linearly related to load. At low loads, the GTO seems more sensitive, but becomes less sensitive at higher loads [9,10].

vi.VA model

Dan Song developed a unified muscle afferent model that included both the muscle spindle and the GTO [10], accounting for all proprioceptive feedback to the CNS.The model uses equations developed by Mileusnic in the previous two studies described. The GTO was simplified to an Ib afferent versus muscle force relationship; the intrafusal fiber models remained unchanged [11].

The muscle spindle and GTO models were combined with a virtual muscle (VM) model, and a SIMM model that calculates joint dynamics based on muscle group activations. The VM model is a musculo-tendon model that estimates extrafusal fiber length and contractile force, and tendon length. Unlike the RQ model, the VM model is a spring-dashpot-contractile element model that does not take into account calcium dynamics and actin-myosin interactions. The VM model is driven by an α motoneuron signal, the muscle spindle is modulated by static and dynamic γ motoneuron signals, the GTO responds to the muscle force, and the SIMM model responds to muscle force and feeds back the new muscle length.

All together, the virtual arm (VA) model, which consists of the three subsystems listed above, is an open - loop model that requires external motoneuron driving signals(see Figure 4). Although this model is able to model single joint and multi-joint movement, and produces realistic neuronal firing rates, it does not explain how motion is planned and how the α and γ motoneuron signals are determined.

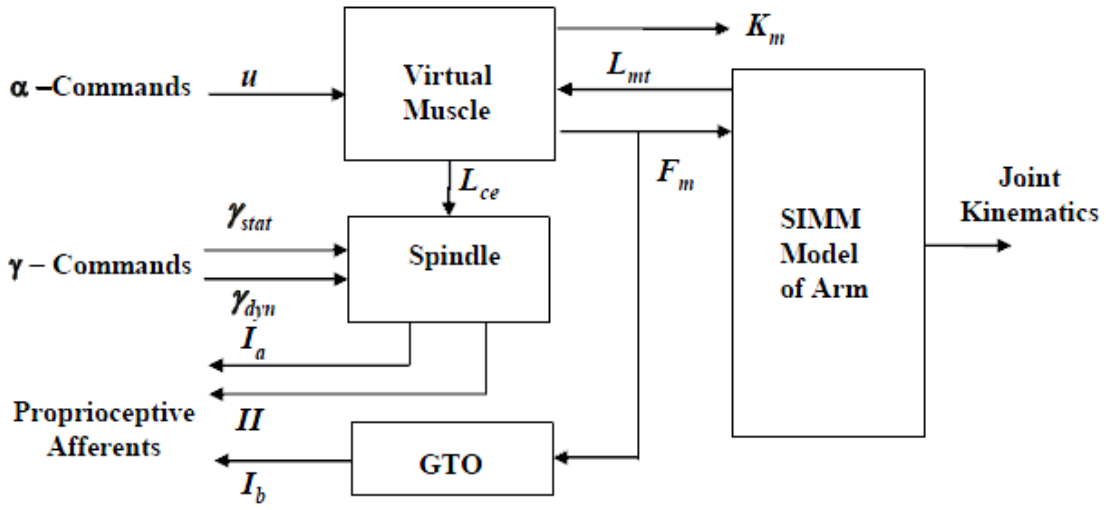

Figure 4: Virtual Arm model consisting of a virtual muscle, muscle spindle, GTO models and the SIMM joint model. This model is open loop since predetermined α and γ motoneuron signal are required to drive it. [11]

vii. α-γ Co-activation and β Motoneurons

During non- isometric tasks, muscle length continuously changes. Therefore, intrafusal fibers must readjust to the new muscle length conditions. Thus process of readjusting intrafusal fibers when extrafusal fibers are shortening is known as α-γ co-activation and is important in proper proprioceptive feedback [4].

There is another type of motoneuron, the β motoneuron that can innervate both extrafusal and intrafusal muscle fibers, but its function is unclear. Maltenfort and Burke hypothesized, in their simulation study, that β motoneurons initiate the α-γ co-activation and are especially important when gamma motoneurons are close to their saturation points [12]. In this case, beta motoneurons can provide an alternate method of control when gamma motoneurons are no longer sensitive (i.e. within their dynamic range). It was also hypothesized that beta motoneurons can be excited by Ia afferents and provide positive feedback to the muscle spindle [13]. Simulations showed that by varying the gain of the positive feedback loop, Ia afferent firing is affected either during lengthening or shortening of the muscle fiber. Unfortunately, beta motoneurons are poorly described compared to alpha and gamma motoneurons, and are usually excluded from muscle models.

viii. Discussion

Physiologically relevantneuromuscular models requires accurate modeling of muscle function. Extrafusal muscle fibers need to respond to alpha motoneuron efferent signals and generate a contractile force; intrafusal muscle fibers need to monitor muscle length and stretch velocity, and respond to gamma motoneuron signals. More complex

models may incorporate the intricate calcium and actin-myosin dynamics seen in theRQ model, however, most established models prefer to use a modified standard linear solid model to describe muscle fiber function.

Movement around a single joint or many joints, is controlled by at least one pair of muscle groups. A joint model would require at least two muscle models, each with an alpha and gamma motoneuron inputs, and Ia, II, and Ib afferent outputs.

II. Joint model

Aside from the muscle models, an accurate joint model must also include tendon and ligament properties. Tendon models are usually included in muscle models since the GTO and Ib afferent function are dependent of muscle - tendon interactions. Ligaments hold the joint together and limit the range of articulation. They account for passive joint properties such as elasticity (stiffness) and viscosity.

In studies by Eldrich, Riener, and Quintern, joint elasticity and viscosity were estimated and modeled for the knee joint [14]. Joint elasticity refers to the amount of restorative torque produced by the ligament at varying joint flexion angles. These studies determined that it can be estimated as a double exponential function seen in Equation 8. Due to the presence of bi-articular muscles, those that span across two joints, the passive elasticity properties of a target joint is influenced by the immediate proximal and distal joints [14,15]. Thus, the angle dependent joint torque is also a function of the proximal and distal joint angles, $\phi_{proximal}$ and ϕ_{distal} , respectively.

$$M_{elast} = \exp\left(c_1 + c_2\phi_{distal} + c_3\phi_{target} + c_4\phi_{proximal}\right) - \exp\left(c_5 + c_6\phi_{distal} + c_7\phi_{target} + c_8\phi_{proximal}\right) + c_9 \quad (8)$$

As seen in Figure 5, contributions of joint elasticity as minimal in the normal range of motion of the joint, but become significant at the extremes of motion. This represents the limiting nature of ligaments that prevents hyperflexion or hyperextension of joints in order to avoid injury.

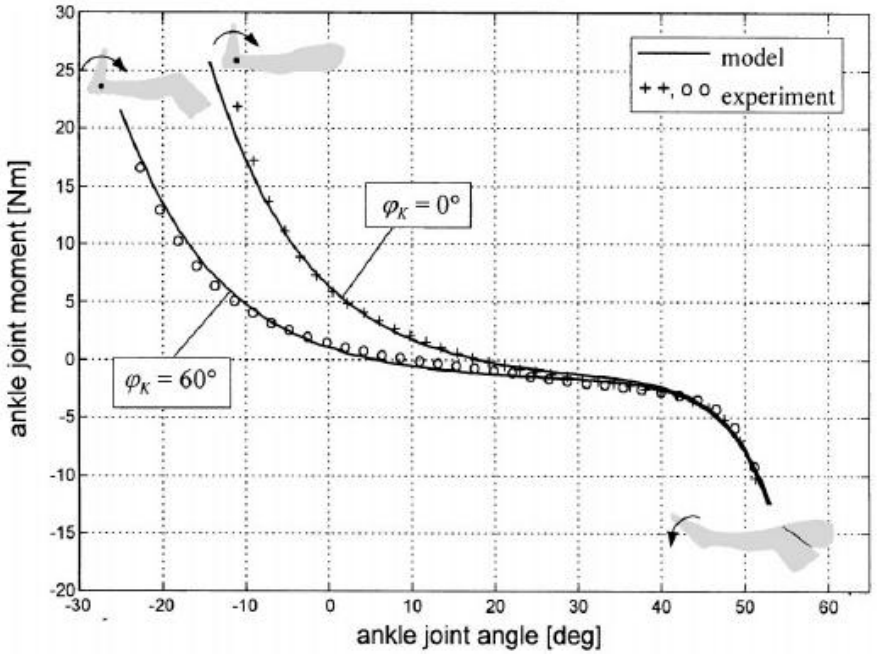

Figure 5: Ankle joint elastic torque at various flexion angles, and a two different knee flexions (φ_k). Passive joint torque is depended on distal and proximal joint conditions. [15]

i. Single joint model

Using the passive joint properties and extrafusal muscle properties, discussed previously, Ferrarin et al. developed a single joint model for the knee to predict knee flexion angle based on an input PWM stimulation signal, which represents α motoneuron function [16]. Again, as was seen in Dan Song's model, this model is open - loop.

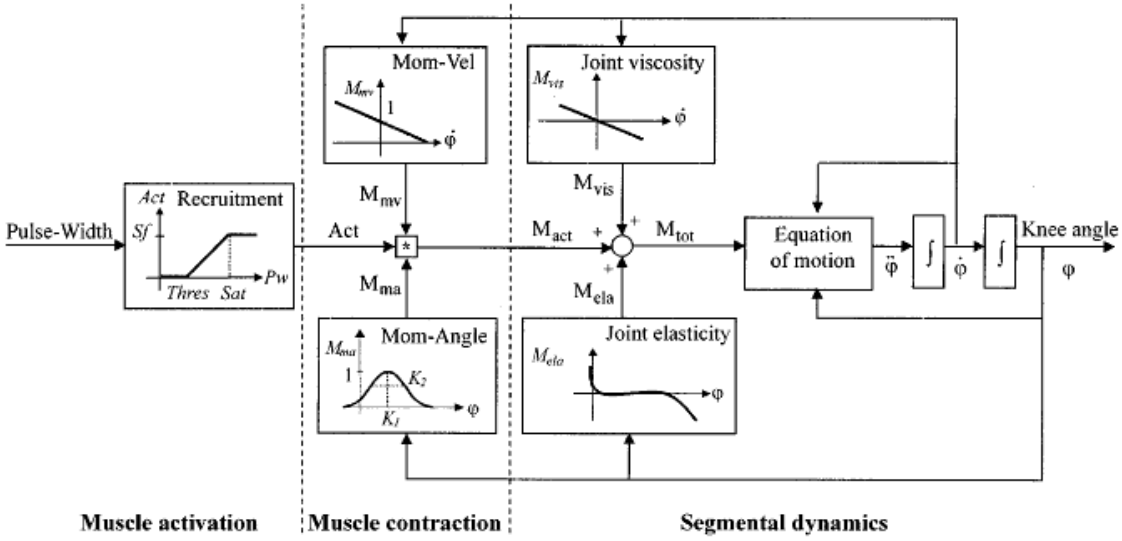

Figure 6: Single joint model relating an input muscle stimulation pattern to the produced joint motion. This model consists of the muscle activation stage that models isometric force generation, muscle contraction stage that models force - length and force - velocity properties of a contracting muscle fiber, and a segmental dynamics stage that models passive joint properties and effects of external forces. [16]

Figure 6 shows the block diagram representation of this model. It consists of a muscle activation stage (described in the Muscle section), a muscle contraction stage, and segment dynamics stage. The muscle activation stage outputs the generated isometric torque due to stimulation. Since flexion and extension are not an isometric tasks but usually isotonic tasks, the generated torque is modified by the force-length muscle property and its viscoelastic properties. These are modeled in the muscle contraction portion. The force-length relationship is represented as a Gaussian curve, centered on the un-stretched muscle length. The center and width of this function are estimated from literature or can be empirically determined [16]. Viscous properties of the muscle where modeled as a linear function relating muscle force to angular velocity. The slope was estimated from literature as it is difficult to test for experimentally. Both of these muscle properties modified the generated isometric muscle torque. This represents the active joint torque. The segment dynamics stage further includes passive joint torques caused by joint elasticity and joint viscosity. This stage also accounts for any external forces that act

of the limb and joint of interest, such as gravity. The combination of these three stages represents most of the muscle and joint properties that affect single joint movement.

The knee joint model consists of three mono-articular and two bi-articular muscle groups that are involved in flexing around the knee. Since this model was open - loop, stimulation patterns for each muscle group can be pre-calculated, or back - calculated using an inverse model. However, this does not explain how the CNS optimally determines activation patterns, especially when more than two muscle groups are present.

ii. Multi-joint model

Riener and Fuhr developed a multi-joint model using similar principles, for a standing up from sitting position task [17]. This task required coordination of hip, knee, and ankle joints, as well as the upper body. Hip, knee and ankle joints were simulated using three single joint models. These joint models are not independent since, as was stated previously, immediate proximal and distal joint affect passive joint properties of the target joint. This mechanical phenomenon is known as joint coupling. It has been proposed that joint coupling can be analyzed by regressed phase plane analysis [18]. Joint trajectories of two joints can be plotted against each other to reveal a correlation plot, an example of which is seen in Figure 7. The R^2 value of this plot describes the strength of coupling between the two joints.

However, it is still unknown how the CNS determines how to control coordination of multiple joints during a complex movement. This is known as the Bernstein redundancy problem: how does the CNS coordinate many degrees - of - freedom (DOF) to accurately execute a motor plan [19]? Solutions to this question often

suggest the use of dimensionality reduction, or optimization, and use complex algorithms such as machine learning or Bayesian inference [19].

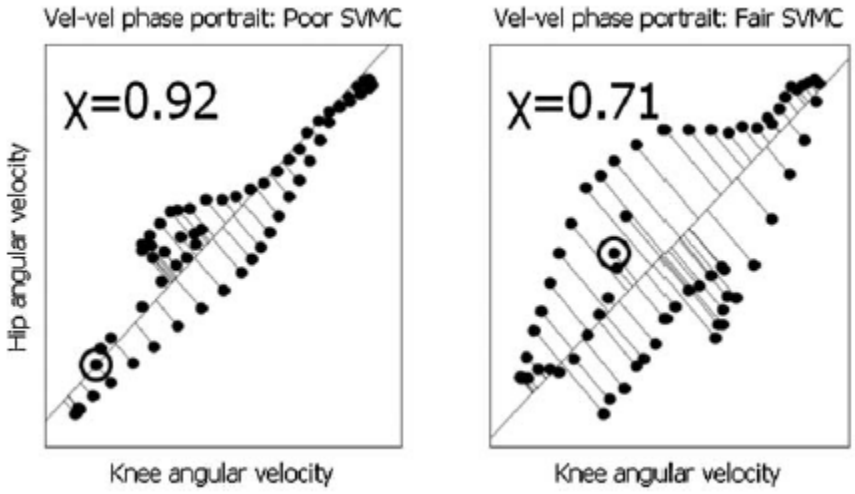

Figure 7: Joint coupling phase plots. Larger correlation between joint velocities indicates a higher degree of joint inter-dependency. [18]

iii. Discussion

A physiologically relevant model should model the passive joint properties caused by ligaments. Many accurate joint models are available for use, and can be incorporated into a neuromuscular control model. These include SIMM, MSMS (an extension of the VA model discussed above), Any-Body and others [19]. Joint and muscle dynamics have been well understood and mathematically expressed. Muscle and joint control, on the other hand, is poorly understood, although many computational control models exist.

III. Involuntary CNS

Descending pathways relay motor plans from the cerebral cortex to the muscle through the brainstem, cerebellum, and the spinal cord. Motion planning does not occur in the descending pathways, but they are critically important in regulating the execution of those plans.Descending pathways also regulate coordination between agonistic and antagonistic muscle groups.

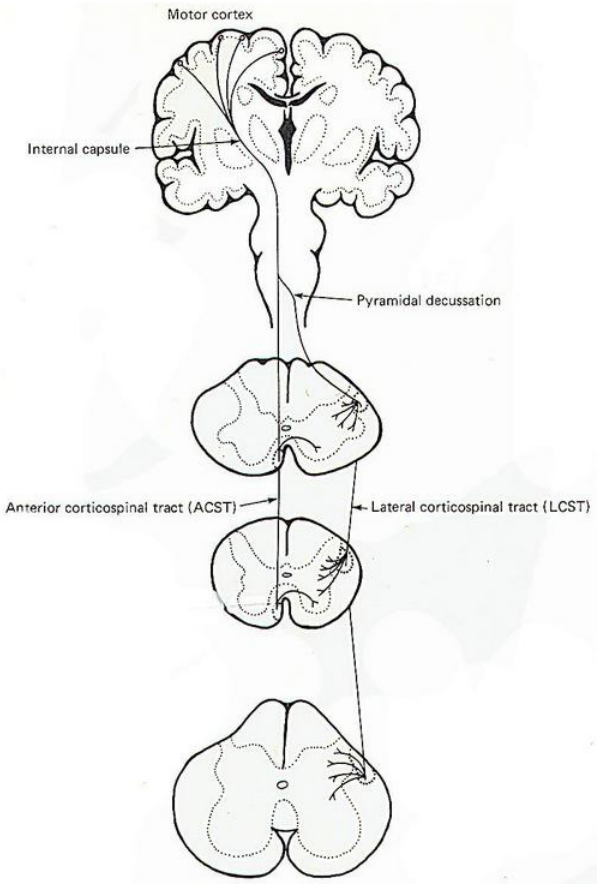

Figure 8: Diagram of the cortico-spinal tract. The lateral CST decussates in the brainstem, while the anterior CST decussates in the mid-thoracic region of the spine. [22]

Several neuronal tracts comprise the descending motor pathways. The main tract is the corticospinal tract (CST) also known as the pyramidal system [4,20]. Motor commands from the primary motor cortex (M1) are relayed to the brainstem, through the spine, and finally to motoneurons. Besides exciting motoneurons, the CST is responsible for reflex responses, gating sensory inputs, and undergoing long term spinal plasticity.

CST nerves receive a majority of their inputs from M1, but also some inputs from the supplementary motor area (SMA), pre-motor cortex (PMC), and sensory cortex (S1). These areas are located mostly in the pre-centralgyrus of the cerebral cortex. When the nerves reach down to the medulla oblongata, 85% of them decussate to the contralateral

side. Decussated nerves then continue down through the brainstem and down the spine; these nerves make up the lateral CST. Non-decussated nerves descend down the ipsalateral side of the spine and decussate at the mid-thoracic region to the contralateral side. When the nerves reach the correct spinal segment, they will often interact with spinal interneurons before exciting motoneurons. Figure 8 displays a diagram of the CST pathway.

Spinal segments are subdivided into three zones: dorsal horn, intermediate zone, and ventral horn [20]. The dorsal horn is responsible for receiving sensory input. Spindle afferents, Ia, II, and Ib, terminate in this region; their signal is ascended up to the cerebellum, but is also processed by interneurons in the intermediate zone. These interneurons are responsible for generating reflexes that are crucial for fast response, and coordinate agonist and antagonist motor commands [20,21]. The ventral horn contain motoneurons that deliver modified motor commands to muscle fibers.

Another important descending motor pathway is the rubrospinal tract. Unlike CST this tract originates in the brainstem, and is known as the extrapyramidal system [4,21,22]. The rubrospinal tract takes input from the red nucleus which receives its inputs from regions of the cerebellum and basal ganglia. Studies have shown that in humans, the mature CST inherits many of the functions that the rubrospinal tract is responsible for in early stages of life [21,22]. It is considered that in the mature nervous system, the rubrospinal tract acts like a redundant pathway for the CST in case damage occurs.

The rubrospinal tract function closely with the reticulospinal pathways (RST). This pathway originates in the reticular formation in the brainstem, and is responsible for further controlling alpha and gamma motoneurons [21,22]. The reticular formation takes

inputs from the motor cortex and cerebellum. Other less studied tracts include vestibulospinal tract, the interstitiospinal tract, and the tectospinal tract [22].

Many of the descending motor pathways receive inputs from the cerebellum. Anatomically, the cerebellum is part of the cerebral cortex located on the dorsal side of the brainstem. It takes input from many regions of the brain, not just the motor cortex and is responsible for learning, attention, motor control, and many other poorly understood functions. Properties of the cerebellum will be discussed further in this section.

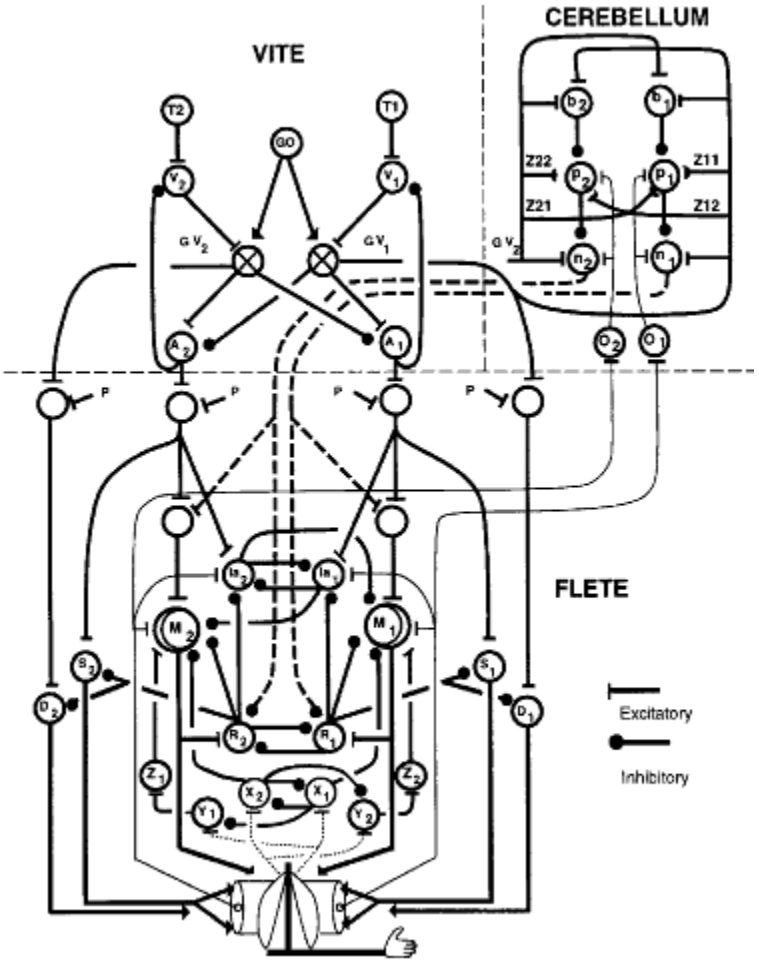

Figure 9: VITE-FLETE-CBM diagram. VITE subunit models the generation of motor commands by the primary motor cortex. FLETE models the function of the brainstem (red nucleus) and spinal interneurons. FLETE also models generation of motoneuron signals, afferent signals, and muscle contraction dynamics. CBM models the learning function of the cerebellum in response to motor errors. [23]

i. VITE-FLETE-CBM (Part 1)

Contreras, Grossberg, and Bullock developed a neural network model of the motor cortex, descending pathways, and cerebellum that is physiologically relevant and can predict some motor disabilities [23]. The model consists of three subunits: VITE, FLETE, and CBM. A diagram of the complete model is seen in Figure 9.

The VITE (vector-integration-to-endpoint) model is the original single joint trajectory predictor developed by Bullock et al [24]. Single joint point-to-point movement is characterized by a bell shaped like joint angular velocity, and a sigmoid-like joint angle trajectory. The VITE model aims to reproduce these results. It has been slightly modified to represent the function of the primary motor cortex in the current model.

As stated previously, M1 is responsible for execution of motor plans and for relaying those motor commands to the descending motor pathways.Motor commands are required for both agonistic and antagonistic muscle groups; coordination of these plans occurs in the spinal pathways.Motor plans, in the VITE model, are represented as a target position vector, Ti, for each muscle group. The initial target position vector always corresponds to the current position of the limb; while the subsequent target position corresponds to the desired motion target. In this way the target position vector can simply be viewed as a step function. VITE is governed by the following equations (Eq.9 - 11):

$$G(t) = G_0 * \frac{(t - t_0)^2}{0.5 + (t - t_0)^2} * u(t - t_0) \tag{9}$$

$$\frac{dV_i}{dt} = 30 * (-V_i + T_i - A_i) \tag{10}$$

$$\frac{dA_i}{dt} = G[V_i]^+ - G\left[V_j\right]^+ \tag{11}$$

Variable G(t) refers to basal ganglia gating of the motor plans (this will be discussed in the next section). It is modeled as a sigmoid function and thus, allows for smooth motion initiation.V_i refers to the difference vector, which computes the difference between the target position and the current perceived position, Ai. It is assumed that this function occurs in the posterior parietal cortex.The high gain on this state equation displays the sensitivity of the difference vector, and possibly instability. It has been proposed that the cerebellum aids in stabilizing the difference vector, essentially "fine tuning" the motor commands. Calculation of the perceived position vector is performed in the primary motor cortex, and represents the first set of motor commands that will be updated and modified by the descending motor pathways. It can be seen from Equation 11, that the perceived position is a function of difference vector for both agonist and antagonist muscle groups. The function $[\ ]^+$indicates that only positive values are realized. dA_i/dt represents the rate of change of the perceived position vectors, which is also known as the desired velocity vector.

Descending pathways and muscle dynamics are modeled in the Factorization of Length and Tension model, FLETE.Specifically,this model reflects the activities of nucleus interpositus cells (NIP), the red nucleus (RN), Renshaw cells, other interneurons, alpha motoneurons, gamma motoneurons (dynamic and static), muscle spindle afferents, extrafusal fiber recruitment, and force generation.

Muscle dynamics are represented with the following equations: (Eq.12 - 16)

$$F_i = k * [(L_i - \Gamma_i + C_i)^+]^2 \tag{12}$$

$$\frac{dC_i}{dt} = \beta_i * \left((B_i - C_i) * M_i - C_i\right) - \ (F_i - \Gamma_F)^+ \tag{13}$$

$$\frac{d^2\theta}{dt^2} = \frac{1}{I_m} * \left(F_1 - F_2 + F_e - \frac{nd\theta}{dt}\right) \quad (14)$$

$$\beta_i = 0.05 + 0.01 * (A_i + n_i + P + E_i) \quad (15)$$

$$B_i = 0.3 + 3 * (A_i + n_i + P + E_i) \quad (16)$$

Variable Fi is the estimation of muscle force and is a function of muscle length - L_i, resting length - Γ_i and contraction dynamics - C_i. Contraction dynamics, in equation 13, are shown to depend on muscle fiber recruitment and on the alpha motoneuron signal, M_i. This is similar to the muscle recruitment mechanism in the Riener and Quintern'sextrafusal muscle model. B_i describes the number of muscle fibers recruited, while β_i reflects the contractile rate or frequency of stimulation. These values are also dependent on the output of the NIP and RN (n_i), and a muscle spindle feedback signal, E_i. It is not specified which afferent E_i represents, but it can be assumed that it is related to the II afferent.Variable P is a co-activation signal, which innervates both the agonistic and antagonistic neuron groups, equally. Co-activation of opposing muscle groups provides stability to the joint and quickly dampens motion.

Spinal segment dynamics are described in Equations 17 - 35. These include excitation of alpha motoneurons, M_i, and excitation of dynamic and static gamma motoneurons, D_i and S_i, respectively. These occur in the ventral horn of the spinal segment.

Interneurons in the intermediate zone are also modeled. Included are Renshaw cells, which dis-inhibit antagonist alpha motoneurons and limit agonist alpha motoneuron firing rates. These functions stabilize the joint and protect it from damage due to tetanus (prolonged contraction of muscle fibers).

$\frac{dR_i}{dt} = (5B_i - R_i)z_i M_i - R_i\left(0.8 + R_j + 25n_i\right)$	(17)	$R_i = [R_i]^+$	(18)
$\frac{dM_i}{dt} = (\lambda B_i - M_i)\left(A_i + n_i + P + E_i + Z_j^+\right) - (M_i + 1.6)(0.2 + R_i + X_i + I_j^+)$	(19)	$M_i = [M_i]^+$	(20)
$z_i = 0.05 * (1 + M_i)$	(21)		
$\frac{dI_i}{dt} = (10 - I_i)(A_i + P + E_i) - (I_i + 1)(1 + R_i + I_j^+)$	(22)	$I_i = [I_i]^+$	(23)
$\frac{dX_i}{dt} = 0.2(5 - X_i)F_i - X_i\left(0.8 + 0.2X_j\right)$	(24)		
$\frac{dY_i}{dt} = 0.2(5 - Y_i)F_i - Y_i(1 + X_i)$	(25)		
$\frac{dZ_i}{dt} = 0.2(5 - Z_i)Y_i - Z_i$	(26)	$Z_i = [Z_i - 0.2]^+$	(27)

Equations 17 and 19 describe the feedback behavior between ipsalateral alpha motoneurons and Renshaw cells. Alpha motoneurons excite Renshaw cells which then inhibit further motoneuron firing. This is indicative of a negative feedback loop control system. Equation 17 also describes the feedback between opposing Renshaw cells. Excited Renshaw cells controlling the agonist group, inhibits Renshaw cells of the antagonist group; this also disinhibits the antagonist motoneurons, causing co-contraction. Equations 18 and 20 specify that outputs from Renshaw cells and motoneurons can only be excitatory.

Ia(I_i) and Ib (X_i) afferent signals are described by equations 22 and 24, respectively. It can be seen that antagonist afferents inhibit the agonist afferent responses. Equations 25 - 27 describe interneuron activity that is also responsible for reflex responses. One important reflex is the myotactic or stretch reflex, which opposes sudden, involuntary, stretching of a muscle. The stretch reflex, causes activation of agonist

motoneurons to oppose the stretch, and inhibition of antagonist motoneurons to relax the antagonist muscle group. Describing the entire flow of excitatory and inhibitory signals may be time is unnecessary. The stretch reflex would initiate with an increase in Ib activity in the stretched muscle group. One can validate that the reflex would, in fact, occur by following the logic of the equations above.

$\frac{dS_i}{dt} = 5(2 - S_i)(A_i + P) - (S_i + 1.2)\left(0.2 + \frac{0.3R_i}{0.3 + R_i}\right)$ (28)	$S_i = [S_i]^+$ (29)
$\frac{dU_i}{dt} = (2 - U_i)S_i^+ - U_i$ (30)	
$\frac{dD_i}{dt} = (8 - D_i)(100G[V_i]^+ + P) - (D_i + 1.2)(1 + 100G\left[V_j\right]^+ + \frac{0.5R_i}{0.3 + R_i})$ (31)	$D_i = [D_i]^+$ (32)
$\frac{dN_i}{dt} = 0.1(2 - N_i)D_i^+ - 10N_i$ (33)	
$\frac{dW_i}{dt} = (2 - W_i)((U_i + L_i - \Gamma_i)^+) - G_v\left(\left(N_i + \frac{dL_i}{dt}\right)^+\right)^{0.3} - 10W_i$ (34)	$E_i = G_s * W_i$ (35)

Equations 28 and 31 describe static and dynamic motoneuron activity. Equations 30 and 33 describe intrafusal fiber contraction due to gamma motoneuron activation. U_i is the contraction of bag_2 and nuclear chain fibers, while N_i represents contraction of bag_1 fibers. Equations 34 and 35 describe the generation of the II afferent signal.

The models of extrafusal and intrafusal fibers is not as complex as those presented by Riener and Mileusnic. Incorporation of those models in the FLETE model would be

useful in improving physiological relevance. However, the VITE and FLETE models have been shown to be closely related to the neurophysiology of motor pathways.

ii. Cerebellum

The cerebellum is a complex brain structure that integrates inputsfrom the brainstem and spinal cord [25]. It is structurally and functionally different from the cerebral cortex. Unlike the cerebral cortex, the cerebellum has a three layer cortex and a deep internal core. The three cortex layers are: the outer synaptic layer (molecular layer), the Purkinje layer, and the inner receptive layer (granular layer). Inputs to the cerebellum are the climbing fibers which originate from the brainstem, specifically the inferior olivary nucleus, and mossy fibers which originate from the spinal cord [25,26,27].Figure 10 displays a diagram of the cells and neuron fibers present in the cerebellum.

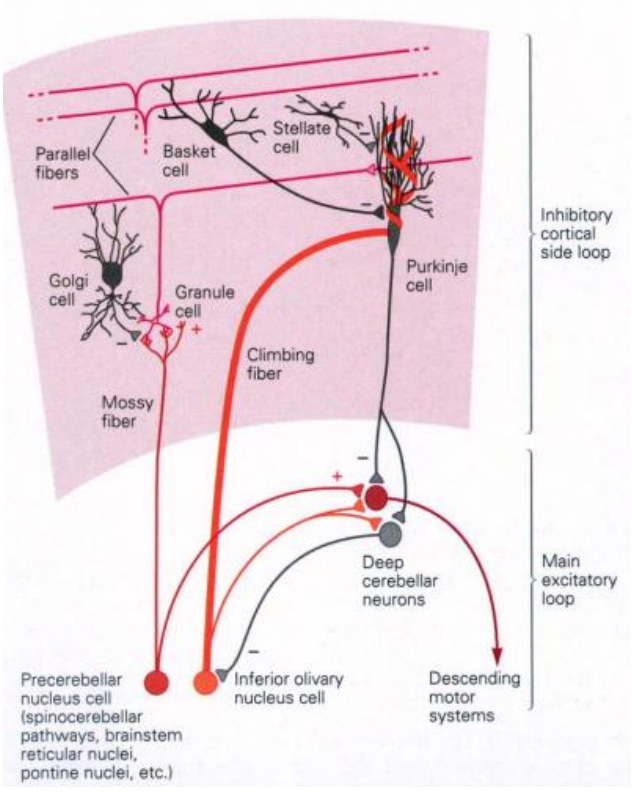

Figure 10: Basic laminar structure of the cerebellum. Mossy fibers bring afferent signals to the cerebellum, which capture motor error. Inferior olivary nucleus cells teach Purkinje cells the expected motor commands. In response to motor errors, Purkinje cells modify outgoing motor commands to reduce those errors [27]

The cerebellum also contains three major functional regions: vestibulo-cerebellar, spino-cerebellar, and cerebro-cerebellar. All are related to motion planning and execution. Spino-cerebellar region is important in receiving sensory afferents directly from the spinal cord and providing an

alternate processing pathway. Often this pathway is responsible for fast response time, that otherwise would not be possible via the CST. Sensory inputs from the spine, brought up by mossy fibers, are integrated by Purkinje cells and relayed to the deep cerebellar nuclei. Climbing fibers from the inferior olivary body also are integrated by Purkinje fibers and by deep cerebellar nuclei [27]. The resultant signal from the deep cerebellar nuclei acts as input to the red nucleus [27].

Although, structurally the cerebellum is well understood, there is still poor understanding of the underlying functions. It is believed that the cerebellum aids with motor learning, where signals from the olivary body act as training signals that drive inductive learning in Purkinje cells [26-29]. It has also been hypothesized that Purkinje cells are responsible for accessing and modifying motor memory, possibly another sign of motor learning [29]. The basic, widely accepted, functions of the cerebellum are timing control of various muscle groups and fine-tuning of motor commands [27-29].

iii. VITE-FLETE-CBM (Part 2)

The cortico-spino-cerebellar model, developed by Contreras et al., consists of a third model, CBM (equations 36 - 43), which is an adaptive neural network equivalent of the cerebellum [23]. Adaptive weights between nodes (which represent the different nerve cells) provide this model with learning capacity.

$$\frac{dp_i}{dt} = 2 * \left(-2p_i + (1 - p_i) * \left(25 \sum_k g_k z_{ki} + t_i + \frac{p_i^3}{0.25 + p_i^3} + 0.3 \right) - (0.8 + p_i) * \left(0.1 p_j + b_i \right) \right) \tag{36}$$

$$\frac{db_i}{dt} = -b_i + 3(2 - b_i) * \left(\sum_k (g_k - 0.4)^+ \right) \tag{37}$$

$$\frac{dn_i}{dt} = 2 * (-2n_i + (1 - n_i) * (0.2 + 2500G[V_i]^+) - (0.8 + n_i)p_i) \tag{38}$$

$$\frac{dg_i}{dt} = 2 * (-2g_i + (1 - g_i) * (0.2 + 25000G[V_i]^+) - (0.8 + g_i)l_i) \tag{39}$$

$$\frac{dl_i}{dt} = -l_i + (2 - l_i) * (25000G[V_i]^+[g_k]^+) \tag{40}$$

$$100 * \frac{dz_{ki}}{dt} = g_k * (30(1 - z_{ki}) - 100t_i p_i z_{ki}) \tag{41}$$

$$\frac{dt_i}{dt} = -2t_i + (1 - t_i) * (33.3(t_i - 0.4)^+ + E_i - 33.3t_i(u_i - 0.4)^+) \tag{42}$$

$$\frac{du_i}{dt} = 0.1(-u_i + t_i) \tag{43}$$

Equation 36 describes the activity of Purkinje fibers as they get innervated by mossy fibers (g_i) and climbing fibers (t_i). The Purkinje cells modulate the response of the red nucleus (n_i) which are part of the rubrospinal tract. Variableb_i represents basket cells and l_i represents golgi cells that inhibit granule cells/ mossy fibers.Learning is realized by adaptive weights (z_{ki}) that act on mossy fibers. Equation 41 shows how the adaptive weights change based on inputs from the climbing fibers, granule cells, and Purkinje cells. It has been proposed that climbing fibers provided instructive signals to correct for movement errors. This process would require plasticity of synapses leading to Purkinje cells. Synapse plasticity is reflected as changing adaptive weights on input signals to the Purkinje cells, and is considered to be a method of learning via long-term-potentiation or depression.

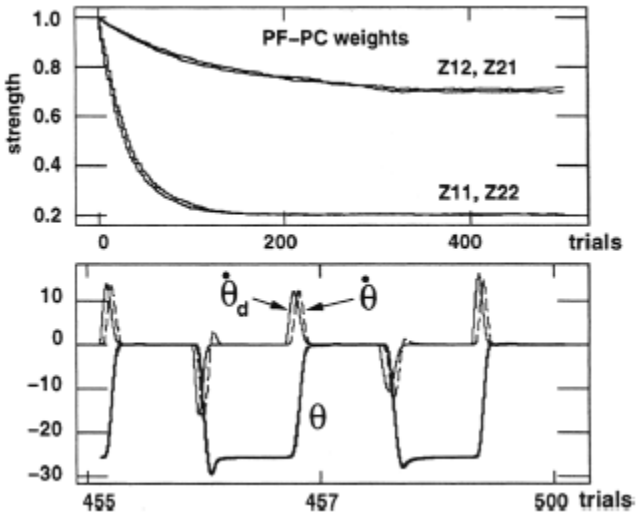

Figure 11: Top: Cerebellar learning causes adaptation of weights between parallel fibers and Purkinje cells. Bottom: after multiple trials, motor errors are consolidated causing produced joint movement to better match the desired joint trajectory. [23]

CBM model results showed asymptotic adaption of weights over multiple simulated motion trials. This adaption caused the actual joint trajectory to match the desired joint trajectory. By reporting movement errors, between the actual and desired trajectories, the cerebellum aided with learning the proper, and novel, motion pattern, previously unseen by the system.Figure 11 shows the adaptive weights over a series of trials and the tracking error between the actual and desired movement trajectory.

iv. VITE-FLETE-CBM Results

Contreras et al., showed the effects of lesions and impairments on motor performance, by removing models or parts of models. By removing the CBM model, the simulation predicted de-cerebrated motions. These motions displayed poor reaction time and slow motion initiation compared to intact movements. Due to the lack of adaptation and learning, the actual joint trajectory did not follow the desired joint trajectory.

Lesions to the CST were also examined. Removing red nucleus projections to alpha motoneurons causes oscillatory behavior throughout the movement. This type of behavior is often seen in cerebellar patients and known as cerebellar tremor [30].

v. CMAC

Many other models of the cerebellum have also been developed. A famous neural network model is CMAC (Cerebellar Model Articulation Controller) [25,31]. This model receive a large input pattern that is then analyzed by parallel logic functions (AND/OR). Weights on inputs and hidden layers are adapted by least mean square error method. This means that a training signal is needed to compare the output of the CMAC model to. Perhaps, the training signal represents the function of climbing fibers and the output of CMAC represent Purkinje cell activation. It is difficult to say, however, since the model is fairly general and not physiologically specific as the one described above.

Wolpert et al. used the CMAC model in a computational model of eye movement due to visual stimuli [31]. They assumed that the cerebellum can be viewed as an inverse model, producing motor commands from sensory input. However, although their model did produce computationally believable results, it is not physiologically accurate. Other studies and model, discussed later, show the complex brain pathways required to produce eye movements due to visual stimuli.

vi. Cortical VITE

VITE, the movement command generator presented in above, is only a functional approximation of the motor cortex and premotor cortex. Bullock, Cisek, and Grossberg improved on the VITE model by identifying phasic and tonic cell types in M1 [32]. Tonic cell types respond continuously to a stimulus, while phasic and phase-tonic cells respond only during the onset of the stimulus [33,34]. This updated model attempts to explain the neural origins of the target position vector, difference vector, perceived position vector, and gating signal, which are all utilized in the original VITE model. The authors also simplified the FLETE and CBM models to test their updated VITE model.

Just as in the original VITE model, production of motor commands originates in the primary motor cortex (Brodmann area 4) and the anterior portion of the parietal cortex (Brodmann area 5).This model made several hypotheses: 1. that the difference vector is calculated in Brodmann area 5; 2. the present position vector is also calculated in area 5, and takes into account the difference between spindle afferents (from Brodmann area 2) and the efference copy (outflow position vector); 3. Outflow position vector (OPV) is calculated by integrating the desired velocity vector (DVV) and feedback from the present position vector; 4. Primary cortex has phase-tonic cells associated with force monitoring, and recruitment of muscle fibers to compensate for external loads.Figure 12 shows the flow diagram of the updated VITE model.

These assumptions give rise to more complex equations (Eq. 44 - 49) to describe the function of the primary motor cortex, premotor cortex, and parietal cortex.

$$r_i = \left(T_i - x_i + B^{(r)}\right)^+ \tag{44}$$

$$u_i = \left(g * (r_i - r_j) + B^{(u)}\right)^+ \tag{45}$$

$$\frac{dx_i}{dt} = (1 - x_i) * \left(\Theta y_i + s_j^{(1)}(t-\tau) - s_i^{(1)}(t-\tau)\right)^+ - x_i * \left(\Theta y_j + s_i^{(1)}(t-\tau) - s_j^{(1)}(t-\tau)\right)^+ \tag{46}$$

$$\frac{dy_i}{dt} = (1 - y_i) * \left(\eta x_i + \left(u_i - u_j\right)^+\right) - y_i * \left(\eta x_i + \left(u_j - u_i\right)^+\right) \tag{47}$$

$$q_i = \lambda\left(s_i^{(1)}(t-\tau) - s_i^{(2)}(t-\tau-\Lambda)\right)^+ \tag{48}$$

$$\frac{df_i}{dt} = (1 - f_i)h * k_i * s_i^{(1)}(t-\tau) - \psi f_i * \left(f_j + s_j^{(2)}(t-\tau)\right) \tag{49}$$

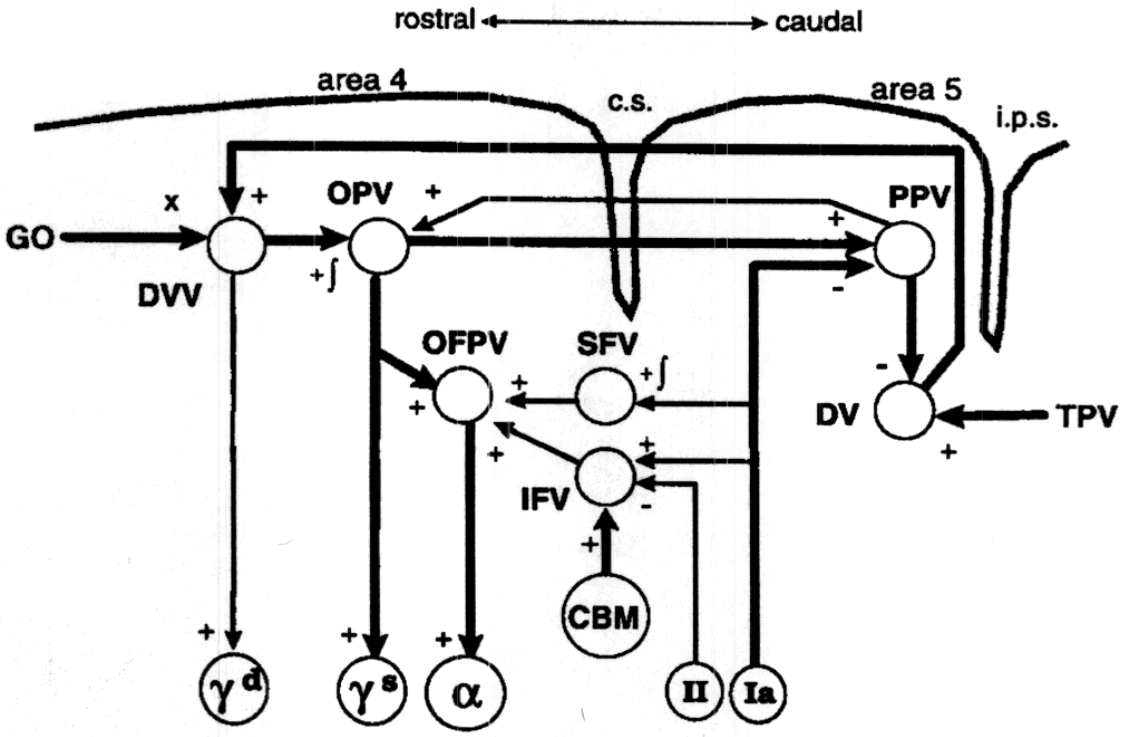

Figure 12: Expanded VITE model that simulates the activities of tonic and phasic cells located in the primary motor cortex (area 4) and the posterior parietal cortex (area 5). OPV represents the generation of the efferent copy that is compared to afferent signals, prior to the computation of the perceived position vector. [32]

Difference vector, r_i, is still calculated as the difference between the target position vector, T_i, and the perceived position vector, x_i. The desired velocity vector (DVV), u_i, is calculated as the gated difference between the DV for agonist and antagonist muscle groups. The efference copy is represented by y_i, and is essentially an integration of the DVV with feedback from the perceived position vector. Equation 46 shows how the perceived position vector is calculated by comparing the efference copy to afferent sensory signals.$s^{(1)}$ is the primary afferent (Ia) transmitted from the primary somatosensory cortex, $s^{(2)}$ is the secondary afferent (II).

Force monitoring is described in equations 48 and 49. The variable q_i represents the inertial force vector (IFV), which looks for differences in limb trajectory caused by

the limb's momentum such as overshooting or delayed initiation of movement. This vector is assumed to be calculated by phasic reaction time cells in the motor cortex, which are a type of phasic cell that responds to the onset of movement. The variable f_i represents the static force vector (SFV) which accounts for external forces such as gravity or an external load. Together the OPV, the IFV, and the SFV produce the output motor commands to the descending motor pathway.

The cortical VITE model makes improvements in characterizing neuronal activity in the cortex, but makes gross approximations about muscle and descending pathway dynamics. This is witnessed in Equations 50 - 57. Simplifications are made in representing afferent spindle signals, and generation of alpha and gamma motoneuron signals. Many spinal circuits, present in the FLETE model, are removed from this model, possibly to reduce the complexity of the overall model and to accentuate the additions to the VITE model.

$$\alpha_i = y_i + q_i + f_i + \delta s_i^{(1)} \tag{50}$$

$$\gamma_i^s = \chi y_i \tag{51}$$

$$\gamma_i^D = \rho u_i \tag{52}$$

$$s_i^{(1)} = S\left(\theta(\gamma_i^s - p_i)^+ + \phi\left(\gamma_i^D - \frac{dp_i}{dt}\right)^+\right) \tag{53}$$

$$s_i^{(2)} = S(\theta(\gamma_i^s - p_i)^+) \tag{54}$$

$$S(w) = \frac{w}{1 + 100w^2} \tag{55}$$

$$M_i = (c_i - p_i)^+ \tag{56}$$

$$\frac{dc_i}{dt} = \nu(-c_i + \alpha_i) \tag{57}$$

Despite the approximations of afferent and efferent signals, and muscle contraction, this model was able to reproduce neuronal firing rates of phasic and tonic cells in the motor cortex and parietal cortex. This validates the improvement of the VITE model, and suggests that further improvements can be done on the FLETE and CBM models.

An independent study tested the cortical VITE model as a controller for a robot finger that used shape memory alloy actuators, as muscles [35]. The model was used to compute proper actuator forces needed to produce point-to-point finger motions. The robot consisted of three joints, thus three instances of the model controlled each joint. Trajectory and velocity plots of the movement resulted in bell shaped velocity profiles indicating that human - like movement behavior was possible with the aid of the VITE model.

IV. Voluntary CNS

The motor system must be able to decide a target to move to, and be able to plan a trajectory that will ultimately lead the limb to the target [36]. Neurophysiological studies have shown that virtually all parts of the brain are necessary for this process. So far the motor pathways described have been relatively involuntary, i.e. they did not plan or decide the motion patterns. Planning and decisions occur in higher brain structures.Prefrontal cortex is necessary for accessing working memory and higher cognitive functions, posterior parietal cortex is necessary for sensorimotor integration, inferior temporal cortex is necessary for sensory information processing, premotor cortex and supplementary motor areas are required for trajectory planning and plan selection, and visual cortices are required for processing visual information [36]. Aside from

cortical structures, subcortical structures are required, as well. Basal ganglia is necessary for switching between plans and initiating movements, and the thalamus is thought to mediate information transfer from cortical to subcortical structures. It is often difficult to establish functional connections between these brain systems due to their complexity.However, many studies have attempted to model their function. Herein, the decision and motor pathways will be described, and crucial brain structures will be examined in detail.

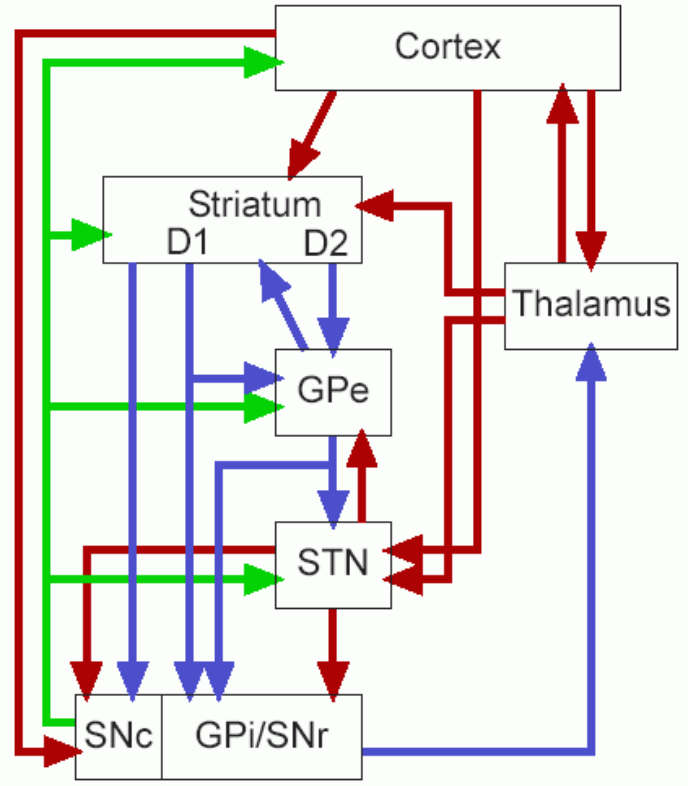

Figure 13: Diagram of the interactions between the cortex, basal ganglia, and thalamus. Green - dopamine stream, which can be excitatory or inhibitory. Red - excitatory glutamate steam. Blue - inhibitory GABA stream. [37]

i. Basal Ganglia

The basal ganglia is a collection of subcortical nuclei located around the thalamus. The basal ganglia receives input from the cortex and then processes the information through a direct and indirect loops that eventually dis-inhibit the thalamus. The thalamus then excites other cortical networks. Communication between nuclei is neurotransmitter dependent. Three types of neurotransmitters are used to excite or inhibit activity: dopamine (excitatory and inhibitory), glutamate (excitatory), and GABA (inhibitory) [37].

Dopamine is produced by the substantia nigra pars compacta (SNc). Deficiencies in dopamine production lead to movement disorders such as Parkinson's disease, caused by the inability to properly initiate movements. SNc provides dopamine necessary for the striatum to process cortical inputs. The striatum is the largest basal nucleus that is composed of the caudate nucleus and the putamen. There is still much debate about the precise role of these two structures, but they are often considered to function together. The striatum receives input from many cortical regions, such as the sensory cortex, limbic system, and prefrontal cortex. The striatum contains GABAergic neurons that have either D1 or D2 dopamine receptors, which differ based on their biochemical pathways in response to dopamine [37,50]. These pathways give rise to the direct and indirect pathways present in the basal ganglia.

Two main structures of the basal ganglia are the globus pallidus internal and external nuclei (GPi and GPe, respectively).GPi receives direct inhibitory input from the striatal D1 neurons and excitatory input from the subthalamic nucleus (STN). GPi outputs inhibitory signal to the thalamus. Thus, the direct pathway is dis-inhibitory. GPe is part of the indirect pathway; it receives inhibitory input from the D2 striatal neurons and inhibits the STN and GPi. Thus the indirect pathway is dis-dis-inhibitory. STN and striatum may receive excitatory input back from the thalamus. A basic flow diagram of excitatory and inhibitory pathways in the basal ganglia is shown in Figure 13. Dis-inhibition of the thalamus allows for execution of motor plans in the motor cortex.

ii. Prefrontal Cortex

The prefrontal cortex is responsible for cognition, decision making, and working memory. It is functionally connected to the basal ganglia, the cerebellum, and nearly all

other brain systems. The PFC synthesizes information from all these regions and coordinates many brain processes. Due to its complexity, the PFC is poorly understood; however, many studies have attempted to understand the underlying properties. fMRI and NIRS has been used to track which parts of the PFC are activated during certain tasks, such as memory tasks, and correlated to the activity of other brain systems [38]. The dorsolateral PFC (DLPFC) is closelyinvolved to motor control. Some studies suggest that the function connection between DLPFC and pre-SMA are responsible for generation of self-initiated movements [39,40]. Studies have shown that self- initiated motion activates the SMA, striatum, globus pallidus, the cerebellum, and the anterior cingulate cortex (ACC) [40]. The ACC functionally connects the prefrontal cortex to the parietal cortex, and aids in selection and timing of movement.

Many cognitive models of the prefrontal cortex exist, ranging from neural networks to Bayesian inference. Since, the anatomical connections of the PFC are so complicated, and poorly understood, these models aim to replicate its cue integration and decision making functions.

iii. Parietal Cortex

The parietal cortex is very important is visual and somatosensory processing, spatial orientation, and visuomotor integration. Output from the parietal cortex most often ends up in the PFC or premotor cortex. The superior parietal lobule and the intraparietal sulcus have been identified as being most significant in controlling visually guided movement [41].

The superior parietal lobule is composed on two major areas: Brodmann area 5 and area 7. Brodmann area 5 has been found to activate the premotor cortex and M1 [42].

This area uses somatosensory information and the efference copy, generated by M1, to estimate the current state of the target limb. Brodmann area 7 is responsible for processing visuo-spatial information [43]. This includes visual transformations, representing the sequences of visual targets, attention shifting among targets. These functions are crucial for visually guided motions, unlike self-initiated motions where the SMA and the PFC generate movement targets [43]. Brodmann area 7 functions closely with Brodmann area 5 and the intraparietal sulcus.

The intraparietal sulcus is comprised of five regions: lateral intraparietal (LIP), medial intraparietal (MIP), ventral - VIP, anterior - AIP, and caudal - CIP. Neurons in the LIP respond most strongly to visual stimuli, and are active during generation of eye saccades. It is hypothesized that the LIP encodes the spatial locations of these visual stimuli in an eye-centered frame [44]. VIP encodes directionality of moving visual stimuli and the distance of that stimulus to the head. Therefore, it encodes spatial locations in a head-centered frame [44]. The MIP encodes somatosensory and visual stimuli in a hand/arm-centered frame [44]. Coordination between these intraparietal regions and the superior parietal areas allows for limb-eye coordination and visually-guided movements [45].

iv. Premotor Cortex and Supplementary Motor Area

Four premotor cortex areas have been identified: PMdr, PMdc, PMvr, PMvc; where 'd' is dorsal, 'v' - ventral, 'r' - rostal, 'c' - caudal. There has been much debate over the function of the premotor cortex studies suggest that it controls many aspects of voluntary motion. A study by Pesaran et al. suggested that PMd plays a role coordinating multiple reference frames monitored by the intraparietal sulcus [46]. During motion,

several reference frames exist: eye - centered target, eye - centered limb, limb - centered target, etc. It is suggested that the premotor cortex aids in comparing these reference frames and extracting necessary location information.

Other studies have suggested that ventral and dorsal premotor cortices regulate muscle contraction patterns [47]. fMRI/ EMG comparison studies showed greater activation in PMd during force generation tasks that require reciprocal activation of antagonist muscle groups. PMv, on the other hand, showed greater activation during fine movement tasks that require coactivation of muscle groups [47]. These results indicate that other possible movement/ task patterns may be controlled by distinct regions of the premotor cortex.

Two other brain regions also are involved with movement generation: the pre-SMA and SMA. Studies have shown that the SMA responds, primarily, during self-initiated, also known as internally generated, movements [48]. The SMA fires prior to the initiation of motion, and is functionally connected to M1. Pre-SMA is less responsible for production of motion, and is more responsible to selecting movement plans and altering current movement plans [49]. It is functionally connected to the prefrontal cortex and subcortical regions such as the basal ganglia. Therefore, the pre-SMA has been found to be active during learning of movement sequences [49]. There is no clear distinction between the pre-SMA and the SMA, since many motor and cognitive functions utilize both regions.

v. Basal ganglia - thalamocortical model

One of the first neuronal models of the basal ganglia was developed by Contreras and Stelmach to explain movement differences between normal and Parkinsonian

movements [50]. The model described in this paper is slightly simpler than the diagram shown in Figure 13. It shows cortical excitation of the striatum, D1 and D2 pathways to the GPi and GPe, inhibition of the STN, and finally the inhibition of the thalamus by the GPi. Feedback from the thalamus to the striatum and the STN is not present in this model. The developed basal ganglia model was coupled with the original VITE model to simulate joint trajectories. In the VITE model, one of the fundamental inputs is the gate signal (G). Previously, it was assumed that the gate signal is a sigmoidal function in time, to allow for smooth initiation of motion. Here, the gate signal is assumed to be the output of the thalamus control by the basal ganglia. Equations 58 - 64 describe the basal ganglia and thalamus functions.

$$\frac{dS_k}{dt} = -A_s S_k + (B_s - S_k)\left(\sum_n I_n + I_{Ach} + \frac{S_k^3}{0.25 + S_k^3}\right) - (D_s + S_k)\sum_{n \neq k} S_k \tag{58}$$

$$\frac{dG_k}{dt} = 2\left(-A_g G_k + \left(B_g - G_k\right)\left(10J_k + \frac{G_k^3}{0.25 + G_k^3}\right) - \left(D_g + G_k\right)(50S_k T_k + 0.2H_k)\right) \tag{59}$$

$$\frac{dH_k}{dt} = -A_h H_k + (B_h - H_k)\left(10J_k + \frac{H_k^3}{0.25 + H_k^3}\right) - (D_h + H_k)(50S_k U_k + 0.2G_k) \tag{60}$$

$$\frac{dJ_k}{dt} = -A_j J_k + \left(B_j - J_k\right)\left(I_k + I_s + \frac{J_k^3}{0.25 + J_k^3}\right) - 10\left(D_j + J_k\right)H_k \tag{61}$$

$$\frac{dP_k}{dt} = 5\left(-A_p P_k + \left(B_p - P_k\right)I_{tonic} - 0.5\left(D_p + P_k\right)G_k\right) \tag{62}$$

$$\frac{dT_k}{dt} = b\left(B_{SP/DYN}(DA) - T_k\right) - cS_k T_k \tag{63}$$

$$\frac{dU_k}{dt} = b(B_{ENK}(DA) - U_k) - cS_k U_k \tag{64}$$

The sum of all cerebral cortex inputs, Ik, cause excitation of the striatum, Sk, but compete with each other via lateral inhibition, seen in the term $-(D_s + S_k)\sum_{n\neq k} S_k$ of Equation 58. In the model k - the number of striatal input is set to 2, to represent D1 and D2 pathways. These pathways co-inhibit each other. The D1 pathway inhibits the GPi, *Gk*, by releasing the dopamine dependent neuropeptide, enkephalin. The enkephalin release dynamics are described in equation 64. It can be seen that the rate of release depends on the levels of dopamine provided by the SNc. D2 pathway inhibits the GPe, Hk, by releasing Substance P and dynorphin neuropeptides. The release dynamics is expressed in equation 63. Again, it depends on the levels of dopamine. Jk represents the activity of the STN, and Pk represents the activity of the thalamus, which is the gating signal in the VITE model.

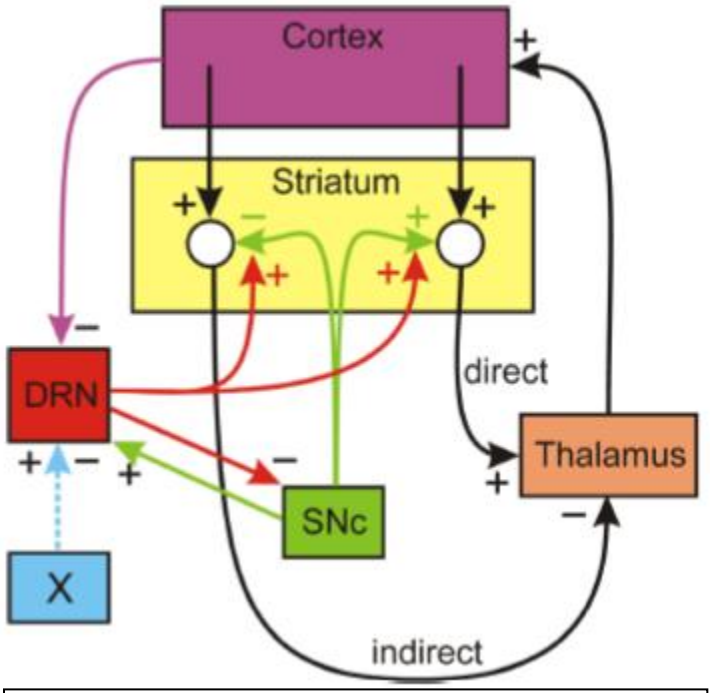

Figure 14: Balancing effect of serotonin on the direct and indirect pathways of the basal ganglia. Cortical modulation of the DRN, affects the activity of D1 and D2 pathways in the striatum. [53]

By varying the amount of dopamine available, the authors simulated normal, slowed, and Parkinsonian movement. Decreasing dopamine levels resulted in an increased reaction time, seen in the longer amount of time required to initiate movements.

It also resulted in longer movement time, seen in lower peak joint velocity and the time to complete the motion. Other studies have corroborated that activity in the globus pallidus is related to the velocity of motion [51]. Increase reaction times are consistent with symptoms of Parkinson's, since patients often have trouble imitating movements. Dopamine levels less that 40% of normal, resulted in akinesia, the inability to produce voluntary motions. Two dimensional tasks such as writing and drawing a line, were also simulated [52]. These showed large distortion of the trajectory during Parkinsonian conditions and slower movement velocity than seen in normal simulations.

Other models of the basal ganglia have been developed to describe the function of certain neurotransmitters. One such model included the effects of serotonin on the production of dopamine by the SNc. Reed et al. hypothesized that serotonin is necessary to create "balance" between indirect and direct pathways in the basal ganglia [53]. Many models, such as the one described above, view the basal ganglia as a closed loop, independent system. However, that assumption is too simple. Regulatory pathways that control basal ganglia function must exist; one such pathway utilizes serotonin. Serotonin is produced by the dorsal raphe nucleus (DRN), which is innervated by the cortical regions such as the prefrontal cortex [53]. Release of serotonin also excites the D1 and D2 pathways in the striatum. Reed et al. created a simplified model of the basal ganglia with DRN control, seen in Figure 14, to monitor the homeostatic effects of serotonin. By innervating the DRN, it is possible to favor either the direct or indirect pathways. Simulations showed that by exciting the DRN, the direct pathway is favored slightly more than the indirect one, and by inhibiting the DRN, the indirect pathway is favored. Excitation of the direct pathway leads to the excitation of the thalamus; excitation of the

indirect pathway leads to the inhibition of the thalamus, thus serotonin can affect selection and execution of motor plans.

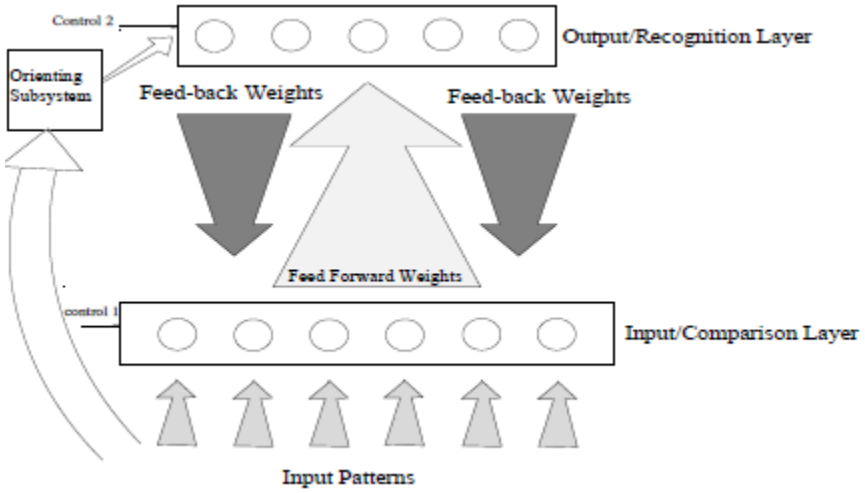

Figure 15: Two layer ART network. The recognition layer contains previously experienced hypotheses. The most relevant hypothesis is relayed into the comparison layer via feedback weights to generate a prototype pattern. If the input pattern matches the prototype vector, the relevant hypothesis is strengthened via feed forward weights. If there is a mismatch, the input pattern generates a new hypothesis that can later be discarded or strengthened. The orienting subsystem monitors whether the input pattern is "close enough" to the prototype vector via a vigilance parameter. [54,56]

vi. Adaptive Resonance Theory

Adaptive Resonance Theory, developed by Grossberg et al., is anunsupervised neural network based model that models memory and decision making [54]. It can be used to model the function of many brain structures including the basal ganglia and the prefrontal cortex. This model differs greatly from generic neural networks.

Many generic neural networks are based on multilayer feedforward topologies. Each node in the subsequent layer connected to every node in the previous layer with certain weights. The activation of each node in the subsequent layer is determined as a weighted sum of every node in the previous layer, thus producing a feedforward weight

matrix, w_{ij}. Additionally, most artificial neural networks require supervised learning to determine the weight matrix. In this case, a training set is used, while the weight matrix is iteratively updated to reduce the mean-squared error between the pre-determined training set output and the current output of the network. Once the weight matrix is determined it remains unchanged during testing.

Adaptive Resonance Theory improves on artificial neural networks to be unsupervised and adaptive. Figure 15 shows the simplest ART network; this network assumes only two layers but can be generalized to have more layers [56].

Unlike general neural networks described previously, ART consists of both feedforward and feedback weights, w_{ij} and z_{ji}, respectively. This allows information to flow, not just from the first layer to the next, but in reverse as well [54,55]. The feedback connection is known as "expectation": the ability of the model to have a certain initial level of expected outcomes that can be modified as new events are encountered.

Initially a certain event is experienced by the system, producing a certain input pattern after sensory processing. This input pattern needs to be recognized and classified as either a previously encountered event or a novel event. The set of previously encountered events, which can be viewed as the set of currently known hypotheses, is contained in the recognition layer (see Figure 15). In order for the input pattern to be recognized it must be compared to the closest matching hypothesis. This operation is performed in the comparison layer. Comparison of the input pattern to the closest matching hypothesis is a complex process that requires feedforward and feedback connection between the two layers, as well as competition within the recognition layer [54,55].

To select for the closest matching hypothesis, the input pattern is initially compared to the current feedforward weight vector for each known hypothesis. This produces a starting level of activation for every node within the recognition layer. Each of these nodes (hypotheses) will compete with each other via Winner-Takes-All (WTA) competition. WTA competition is modeled by on-center-off-surround additive shunting equation which is borrowed from the way ganglion cells are activated (Eq.65). Ganglion cells are excited by central rods, but inhibited by surrounding rods. In the same fashion, each node attempts to promote itself while inhibiting all the other nodes. The node that is least inhibited is considered the winner, and it becomes the "expectation" that will be sent down to the comparison layer.

$$\frac{dx_i}{dt} = -Ax_i + (B - Cx_i)\left[I_i + \sum_{k=1}^{n} f_k(x_k) y_k D_{ki} z_{ki}\right] + (E + Fx_i)\left[J_i + \sum_{k=1}^{n} g_k(x_k) y_k G_{ki} z_{ki}\right] \tag{65}$$

Feedback weights are used to convert the expected, or winning, hypothesis into a prototype vector to be compared to the input pattern. If the input pattern matches the prototype vector "close enough" then the system is set into a state of resonance which promotes long term learning [54,55]. If there is a mismatch, then the system is set into a state of reset which expands the hypothesis set. The parameter that determines whether the match is close enough or not is the vigilance parameter set in the orienting subsystem (see Figure 15). High vigilance parameter promotes generation of a very detailed hypothesis set, while a low vigilance parameter promotes strengthening and learning of a general hypothesis set [54]. This is widely known as the stability - plasticity dilemma that many neural networks face [55]. The system must be plastic enough to incorporate new relevant events into the hypothesis set, but must be stable enough to remember previous

events/ hypotheses if the system encounters an irrelevant event. A relevant event would encounter more evidence over time and will be learned by the system; while an irrelevant event might never be encountered again and should, therefore, be excluded from the hypothesis set. In earlier ART networks, the vigilance parameter was picked as a fixed value, however, new studies developed adaptive mechanisms for the vigilance parameter thereby removing this fixed parameter constraint [57].

As stated before, when the comparison layer determines a match between the prototype vector and the input pattern, the system is put into a state of resonance. In this state, long term learning occurs. The feedback and feedforward weights for that hypothesis node are strengthened since more evidence was just provided for the winning hypothesis.

When a mismatch occurs, this causes the orienting subsystem to reset the WTA competition in the recognition layer. Additionally, a new hypothesis (the current, novel event) is added into the hypothesis set. Any future competition within the recognition layer will now have to include the new hypothesis event. As more evidence for this hypothesis arises, the hypothesis will be strengthened via the adaptive weights. If no more evidence is provided, then the adaptive weights will reduce to zero and the hypothesis will be forgotten.

These two forms of learning techniques are fundamental in modeling human learning behavior. Match based learning, or strengthening of existing hypotheses, is known as the *What* stream [54]. It is important for object recognition and categorization, as well as any other spatially invariant learning. For object recognition, for example, it would be very inefficient if a new hypothesis node were to be created for every new

spatial position and viewing angle of that same object. That would cause cluttering of the recognition layer. Mismatch based learning is the known as the *Where* stream [54]. This stream causes the formation of new hypotheses and the deletion of others. Such learning is important for spatially variant recognition, where the location of an object, but not the object itself, is important. One example of *Where* learning can be seen in limb motion. At each time point, the current position of the limb is important, while the previous positions can be forgotten as they no longer influence the current event. Inability to remove old, irrelevant, hypotheses and to add new, relevant, hypotheses, would lead to cluttering of the recognition layer with duplicate hypotheses. Together these two learning streams explain most of the natural learning that occurs in the brain.

Modifying this basic flow of the ART network can model the functions of individual brain systems more specifically.

vii. TELOS model

Neural origins of eye saccades have been studied in more detail than those of limb motion. Control of eye saccades requires mainly brain systems for voluntary motion, without the regulatory dynamics of the spine and muscle spindles. Motor planning required for eye saccades can be viewed as analogous to that for discrete limb motion.

Brown, Bullock, and Grossberg developed a physiologically relevant model of saccade generations that includes a simple approximation of the visual cortex, the inferior temporal cortex, frontal-eye fields, prefrontal cortex, basal ganglia, posterior parietal cortex and superior colliculus models based on ART [58]. A block diagram of the model is shown in Figure 16.

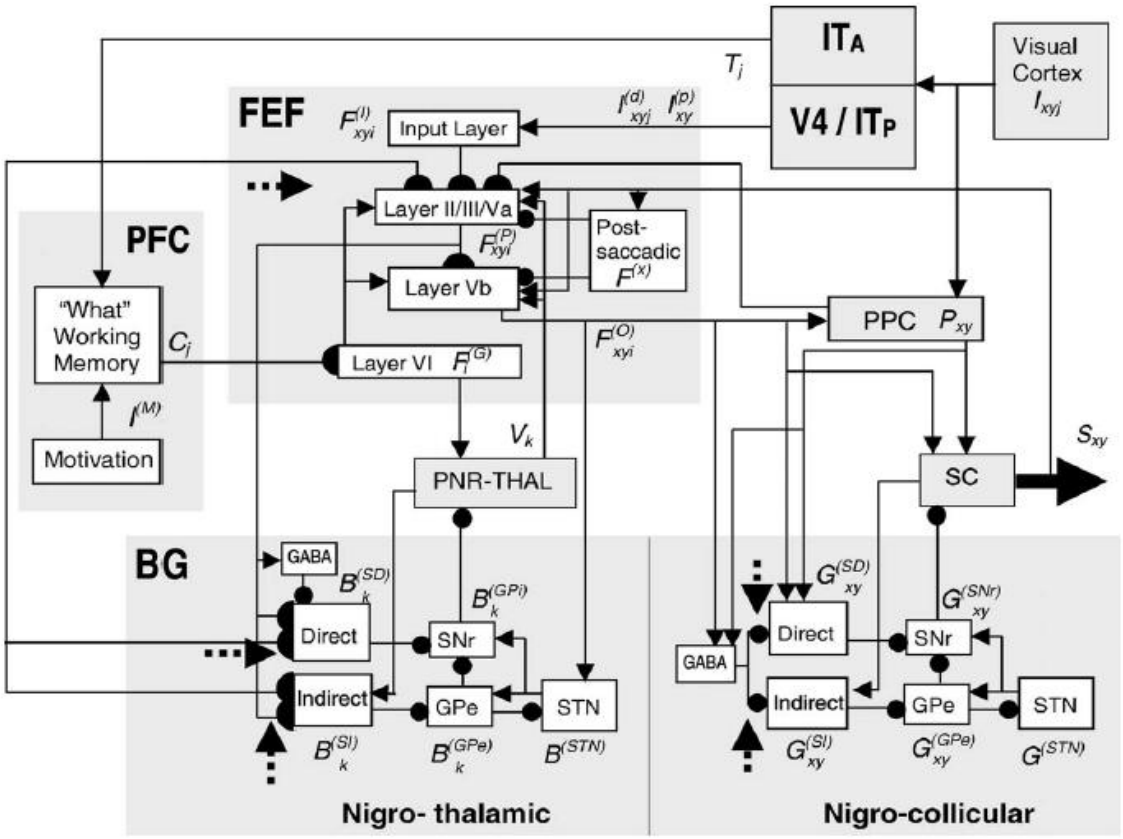

Figure 16: TELOS model. FEF generates saccade plans based on the visual stimuli. Plans compete in the nigro-thalamic basal ganglia. The winning plan is compared to the input pattern generated within the PPC. If the saccade plan agrees with the input pattern in the PPC, the nigro-collicular basal ganglia disinhibits the superior colliculus, thus producing a saccade burst. [58]

Visual stimuli are processed independently by the *What* cortical stream and by the *Where* cortical stream. This operation is done to prevent an explosion of space dependent target representations. The *What* stream, generated by the anterior inferotemporal cotrex (ITa), recognizes the presence of saccade targets (object recognition). The *Where* stream, generated by ITp (posterior IT), identifies spatial locations with particular features. These features can identify a fixation point or saccade target. Fusion of *What* and *Where* streams is performed in the frontal eye field (FEF), which maps the saccade targets and fixation point onto retinotopic coordinates. The model proposed by Brown et al. is a laminar model, which takes into account different functions that are performed by different cortical layers within one brain structure [58]. The FEF, for example, is

subdivided into an input layer, plan layer, output layer, and category layer. These layers work with other brain systems in order to generate saccade plans.

The posterior parietal cortex (BA 7),can be viewed as the comparison layer, while the FEF can be viewed as the recognition layer. Saccade targets and the fixation point compete by simple lateral inhibition (on-center-off-surround) within the PPC, until only one saccade target is chosen. Saccade plans compete with each other, not by simple lateral inhibition, but by exciting the basal ganglia. Only one plan can excite the thalamus, and be realized by the FEF output layer. Comparison of the saccade plan and the saccade target occurs in the nigro-collicular BG loop. A saccade occurs when the PPC and FEF reach coherence, i.e. a resonance state. Figure 17 illustrates the decision behavior of these brain systems when planning a saccade.

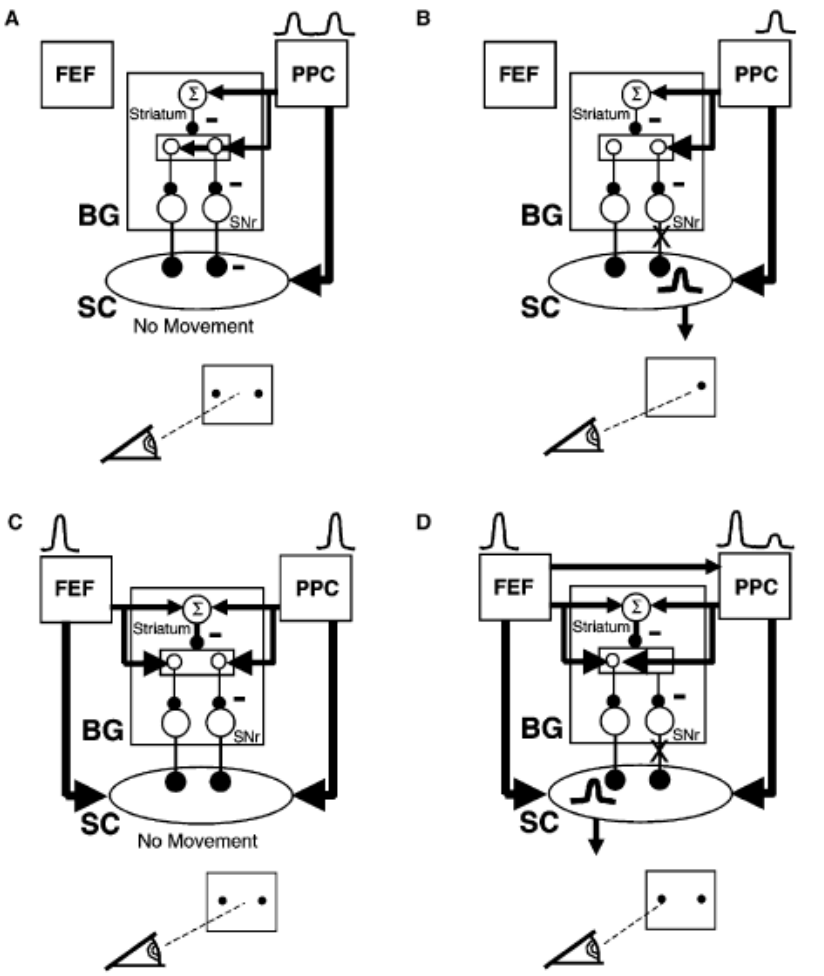

Figure 17: Winning saccade plan from the FEF and the input pattern in the PPC must agree prior to saccade generation. If no plans are present and one saccade target exists, a reactive saccade will be produced. A detailed explanation of the panels in provided in the text. [58]

In panel A, the PPC is presented with multiple saccade targets. This will not generate a saccade since one saccade target has not emerged from WTA competition. When the targets do compete, the winner excites the basal ganglia, thus triggering a saccade, as seen in panel B. In this case the FEF did not present an input pattern (saccade target) that differed from the already know saccade hypotheses in the PPC. This type of saccade is called a reactive saccade, since no prior plan was proposed by the FEF.

Panel C describes the situation when a new plan is presented. In this case, no saccade will initially occur until the novel saccade target is integrated into the set of already know saccade hypotheses. The PPC must recognize this new target as a possible outcome. Over time (several ms), more evidence for the novel saccade target accumulates, mainly since the LED for that target is still on. The adaptive weights adjust for that hypothesis since the saccade target is not irrelevant, and a saccade will happen when the FEF and PPC finally reach a state of coherence, as seen in panel D. This type of saccade is a planned, voluntary, saccade.

The TELOS model makes large improvements in modeling the basal ganglia and cortico-basal connections. This model realizes the funnel structure of the cortico-striatal-GPi: an order of magnitude reduction of neuronal cell between the cortex, striatum, and GPi. The basal ganglia still maintains accurate plan gating function, despite the drastically reduced degrees of freedom (cellular resolution). The model suggests that plans are topographically arranged within cortical structures to allow simultaneous existence of multiple plans without mixing during the "funneling" process of cortico-striatal-GPi connections. Equations derived by Contreras-Vidal and Stelmach, assumed 1:1 neural connection between the cortex and basal ganglia substructures [47]. TELOS assumes 20:1, or larger, ratio of neural connections between consequent basal ganglia structures [58]. Mathematically, this is reflected as a large gain coefficient of the state equations. This uncovers a structural problem, not seen in 1:1 connection models: methods must be in place to deal with saturation of cell activity. The topographic segregation is reflected by competing basal ganglia channels , and the channel that wins, excites the thalamus, releasing the plans for execution.

The basal ganglia model contains a hyper-direct pathway that connects the cortex to the subthalamic nucleus. This provides a direct process to inhibit the thalamus once a plan has been selected and is being executed. Such hyper-direct inhibition ensures that no further movement plans are sent out, until the current plan is executed.

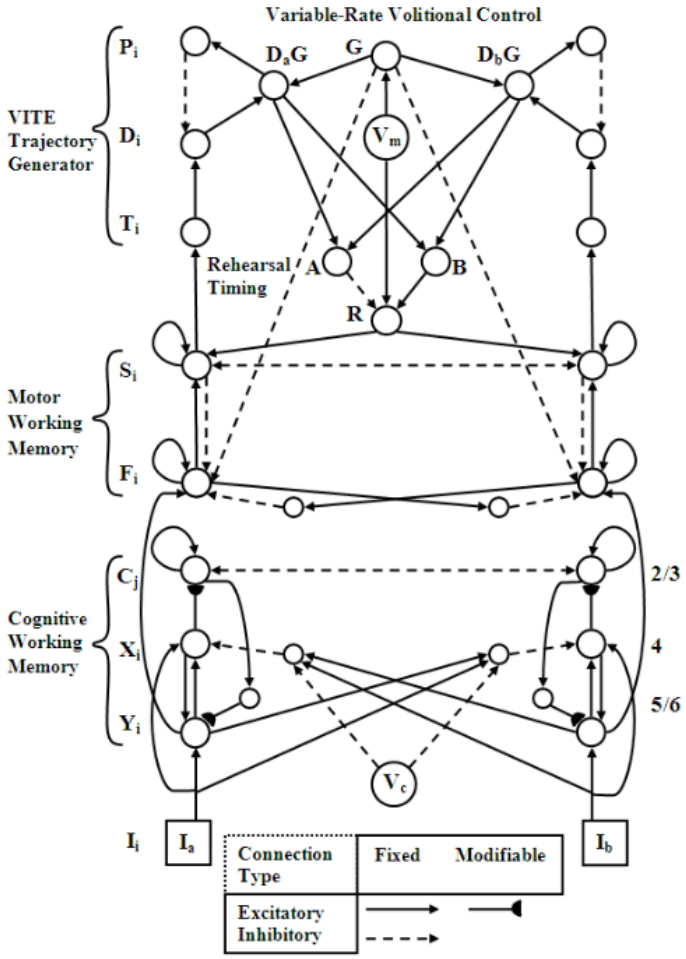

Figure 18: LIST PARSE model that describes the generation of motion to a stored target in working memory. [59]

The TELOS model also contains a PFC subunit to model working memory for storage of stimuli. The working memory model, presented in this study, is very simplified and not representative of all the properties that characterize working memory. This study focused on developing an accurate model of laminar cortex dynamics, and a realistic model of the basal ganglia.

viii. LIST PARSE

The following model, LIST PARSE developed by Pearson and Grossberg, uses ART to represent storage and retrieval of item lists into/from working memory [59]. LIST PARSE models the cortical structure and function of the prefrontal cortex. It

isjoined with a slightly modified VITE model to simulate single joint movement between a series of recalled targets. The complete model is seen in Figure 18.

LIST PARSE consists of a cognitive working memory and motor working memory stages that encode the temporal sequence and spatial locations of a series of inputs. Similar to TELOS, this model simulates functions with in various cortical layers of a target brain system (in this case, the PFC). Due to the nature of ART networks, previously described, new items such as words or actions, can create their own list category, e.g. chunk without interfering with previously learned chunks. Therefore, many stimuli can be encoded into working memory but with a cost to their relative activations. Since working memory is limited in its capacity, long sequences will redistribute the total working memory resources and lower individual chunk activation levels. This leads to two phenomena seen in recall of WM: primacy and recency [59]. Primacy indicates that the first item to be learned acquires the largest activity and further items receive less and less activity. Recency indicates that the last learned item receives more activity than the one before it. These two properties of WM compete to form a "bowed-gradient" activation pattern amongst the stored items: the first and last items receive the greatest amount of activation while the items in the middle receive the lowest amount of activation. This can be shown in a free recall task, where subjects are asked to recall items in any order: first and last items are usually recalled first while items in the middle can be forgotten. Items are recalled from memory in a highest - to - lowest activation fashion.

Cognitive working memory is stored in the ventrolateral prefrontal cortex. It is encoded in layers 4 and 6, and packaged into list chunks in layers 2/3 [60]. Motor

working memory is stored in the dorsolateral prefrontal cortex, where it is read out for motion planning [60]. The dorsolateral PFC works in tandem with the pre-SMA to generate motion plans. Recall of stored items is triggered by a signal from the basal ganglia that sets off a "rehearsal wave". Here, the basal ganglia is simply a step function, switching "on" to trigger recall. The rehearsal wave triggers the recall of the most active item [59,60]. To prevent further recall of the same item, the recalled item inhibits itself, and the activation strengths are renormalized amongst the remaining items.

The VITE model takes the sequential item outputs (items represent a movement target, for example) and generates a movement trajectory. A mechanism must be present to prevent recall of other items while the trajectory is being realized, thus the rehearsal wave must be suppressed until the end of motion. Grossberg and Pearson proposed the presence of Performance Rate Estimator cells that track the velocity of motion at different lag times [59]. The rehearsal wave is restored when these cells determine that the trajectory is nearing its target. Thereby, the selection for the next item begins slightly prior to the end of the previous item's trajectory. This is known as anticipatory movement selection.

LIST PARSE describes how items (targets) are stored and recalled to/from working memory, and how they are selected for trajectory generation. The model, however, makes large approximations and simplifications in terms of basal ganglia function and trajectory generation. Working memory is necessary for motion between multiple targets or selecting for motion between these targets. Variants of LIST PARSE have been applied to eye saccades, speech processing, word recognition, and other cognitive processes.

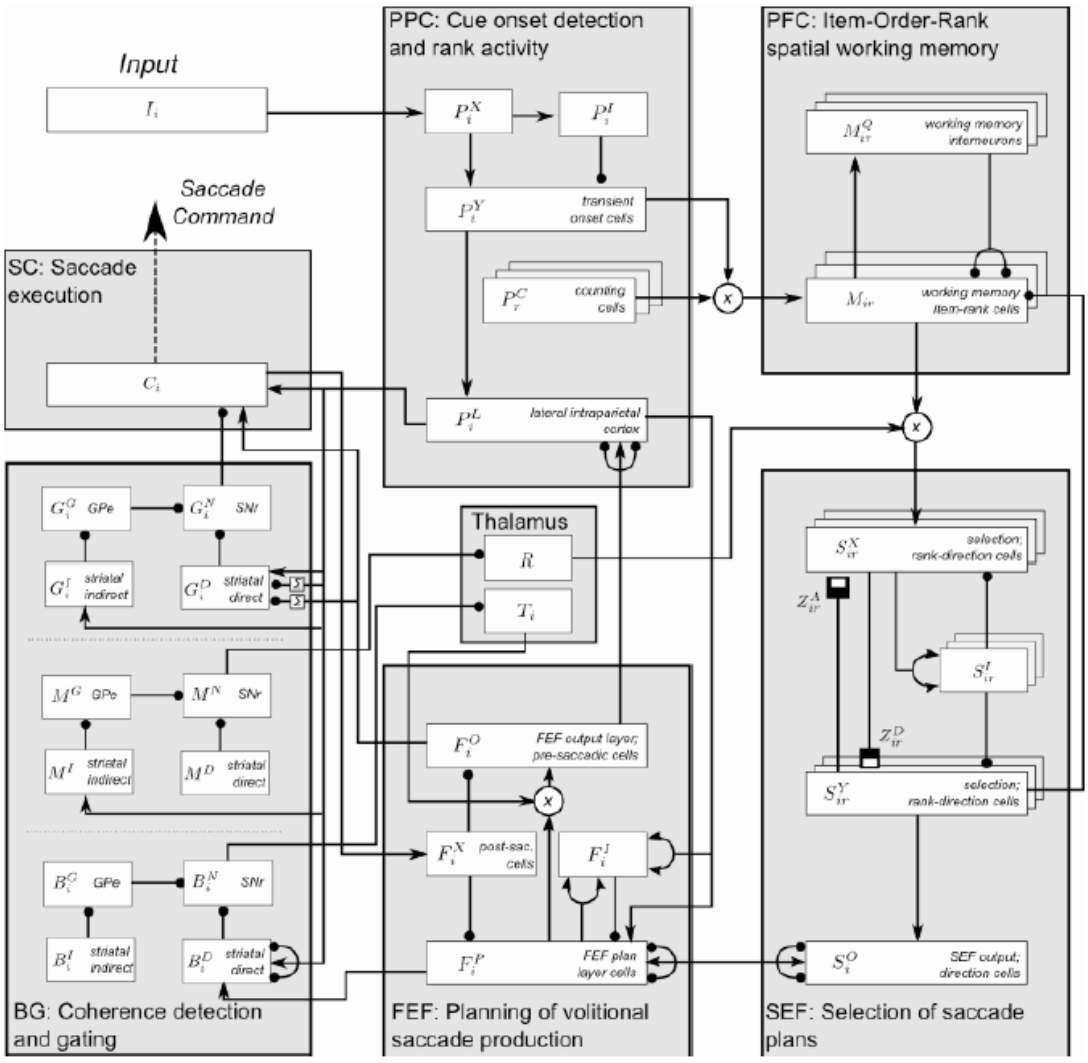

Figure 19: lisTELOS model. This model contains the same features seen in the TELOS model, and working memory properties seen in the LIST PARSE model. [61]

ix. lisTELOS

LIST PARSE and TELOS have been combined by Silver et al. to develop an updated and optimized model of eye saccade generation, known as lisTELOS [61]. This model contains the features of the TELOS and LIST PARSE, and improves upon some of the brain systems. Figure 19 shows the structure of lisTELOS consisting of: the PPC, PFC, selection eye fields (SEF), FEF, basal ganglia, thalamus, and superior colliculus.

Three basal ganglia loops are seen in this model: the working memory loop, FEF loop, and collicular loop. The biggest improvement of the LIST PARSE is the inclusion of a realistic basal ganglia gating model that triggers the rehearsal wave for read out of stored items. In this model, read out of working memory occurs when the visual stimuli are removed. This causes the dis-inhibition of the thalamus, and the saccade targets are read out into the SEF. The SEF works with the dorsolateral PFC to recall most active targets, inhibit them, and renormalize activities of the remaining targets. Unlike in LIST PARSE, where performance-rate-estimator cells monitored completion of movement trajectories to time out recall, in lisTELOS the rehearsal wave does not get modulated. Instead the FEF grabs outputs from the SEF once the FEF post-saccadic cells realize the end of a saccade. The FEF and PPC interactions are identical to those presented in the TELOS model. Again, one basal ganglia loop is required for WTA competition of saccade plans with in the FEF, and a second basal ganglia loop is required to trigger the superior colliculus when the PPC and FEF are coherent.

The PPC is imparted with an additional function of having temporal sensitivity to visual stimuli. This function is realized by rank sensitive counting cells, present in the superior parietal lobule, that modulate the spatial sensitivity of intraparietal cells. This way the temporal sequence of targets is redundantly coded by the PPC and by the PFC in working memory [61].

lisTELOS was used to simulate eye saccades between multiple saccade targets. Saccade cues were placed in a 2D 9x9 grid with the fixation point located at the center. Several tasks were examined; two of interest are the overlap task and the immediate serial recall (ISR) task. In the overlap task a saccade target is presented while the fixation point

is still turned on, requiring a decision to trigger the eye saccade. The ISR task presented a series of various saccade targets while the fixation point of turned on. Once the fixation point was turned off, the subject was to generate saccade jumps to the presented targets, chronologically, from working memory.

Results of the overlap task and ISR task matched results from other saccade decision studies and models, which used Bayesian inference [62,63]. Neurophysiological recording from various brain structures matched simulated activation traces generated by lisTELOS. These results support the validity of these ART based models. Many computational models of brain function exist, however, ART is the closest to simulating real neuronal activity that is require to produce those functions.

Simulation Results and Discussion:

Models were simulated and verified using Matlab and Simulink (*Mathworks*). Several of the model discussed above were simulated individually, and then an attempt was made to combine them.

I. VITE-FLETE-CBM

The original VITE-FLETE-CBM model was developed in Simulink using Equations 9 - 43, as seen in Figure 20. Two of each submodel is present to represent agonist and antagonist muscle groups and motor pathways. Motoneuron signals and joint trajectory were monitored during simulation. Parameters used in the model were similar to those used in the original study; they are listed below.

$\tau = 0;$ $\lambda = 10;$ $z_{11}(0) = z_{22}(0) = 1;$ $z_{12}(0) = z_{21}(0) = 0;$

$P = 0.3;$ $\Gamma_0 = 20.9;$

$I_m = 1;$ $TPV_i(t) = TPV_j(t) = 20;$ $TPV_j(0) = 19;$ $G_0 = 0.001;$

$n = 0.2;$ $TPV_i(0) = 21;$ $\theta(0) = -\frac{\pi}{2};$

$\theta(end) = 0;$

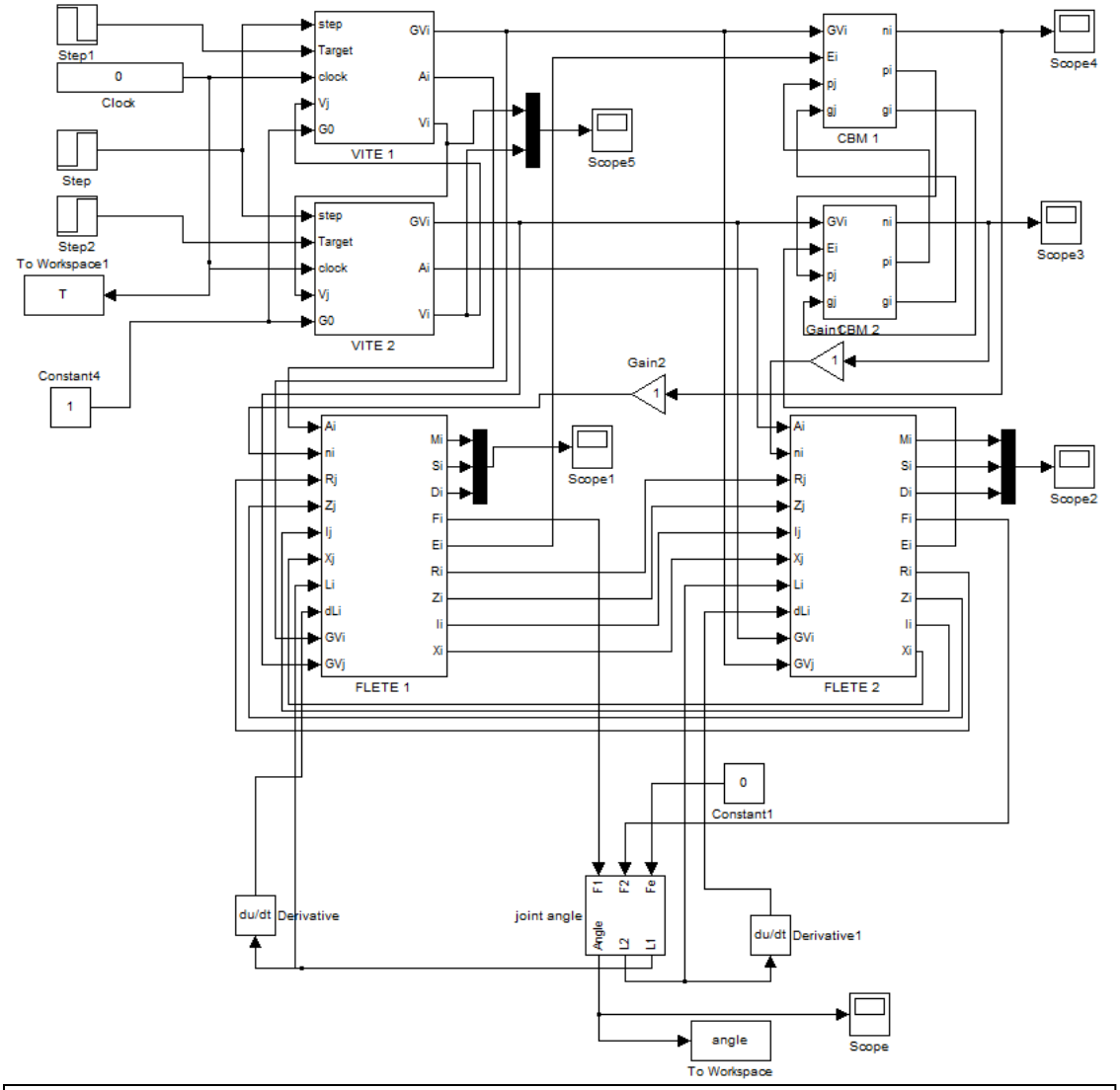

Figure 20: VITE-FLETE-CBM simulink model. Two of each model is present to represent agonist and antagonist muscle control. Alpha motoneuron, static gamma motoneuron and dynamic motoneuron activity is monitored by Mi, Si, and Di, respectively. Agonist and antagonist muscles flex the joint. Afferents monitor muscle length and stretch velocities.

Initially the limb was set to a fully extended position: $\theta = -\pi/2$. The initial target position vector, TPV(0), was thus set to 21cm for the flexor, and 19cm for the extensor. The final target position was a 90 degrees flexed position: $\theta = 0$ in the simulation. Flexor and extensor muscle lengths in this position would be 20cm.Two tests cases were explored: one in which the entire cortico-spinal model was intact, and the other were the cerebellum was disconnected from parts of the model.

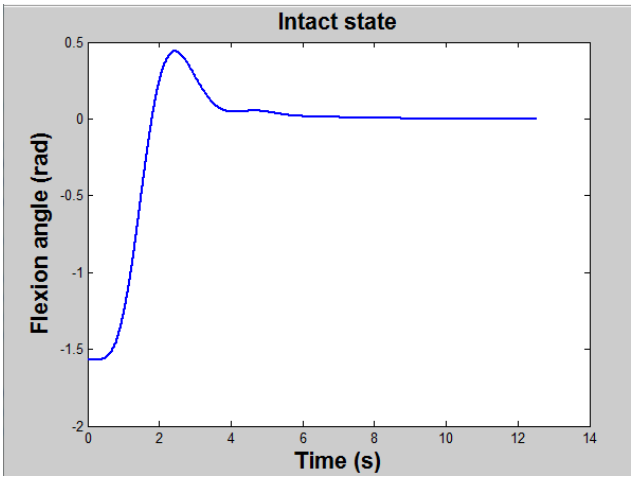

Figure 22: Joint flexion trajectory for an intact model.

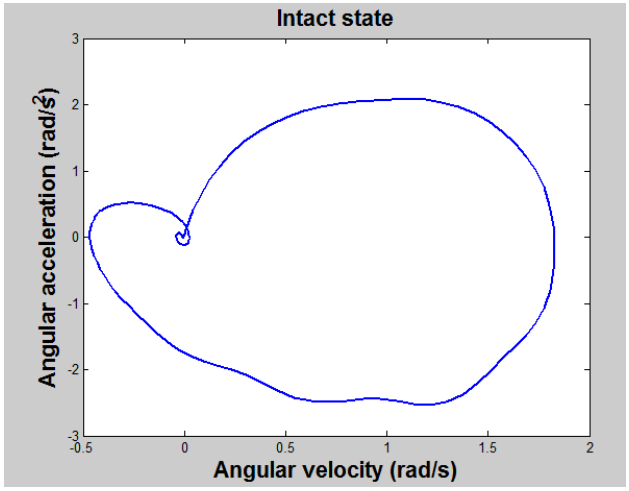

Figure 21: Acceleration-velocity phase plot of the joint trajectory in Figure 21. It is not ellipsoidal, and has large deformities caused by inaccuracies of the VITE-FLETE-CBM model.

Figure 21 displays the joint angle trajectory produced by the intact model. Some morphological features are evident from the plot: the overshoot by a significant value (0.5 rad) and slight oscillations at the end of motion. Phase plane analysis, described in Krasner et al., has been shown to be a good descriptor of the dynamics of motion. Normal discrete motion is characterized by an ellipsoidal trace in the acceleration - velocity (AV) phase plane. The AV phase plane of the joint trajectory

simulated by the model is seen in Figure 22. Clearly, this trajectory is distorted, primarily by the overshoot and the subsequent oscillations.

Removing cerebellar connections to the motoneurons in FLETE, Mi, simulates cerebellar disorder, leading to tremor.NIP/RN projections to Renshaw cells were preserved, therefore the cerebellum can inhibit their activity. The resultant trajectory is seen in Figure 23. In this case, pronounced oscillations occur around the target position, similar to what is seen in cerebellar conditions [30]. This instability is likely due to the inhibited Renshaw cells dis-inhibiting the alpha MN pool causing high gain excitations. These results display the functional importance of the cerebellum in creating responsive and smooth motions that are otherwise impossible. Indeed, patients with cerebellar disease experience persistent tremor as seen in the impaired results.

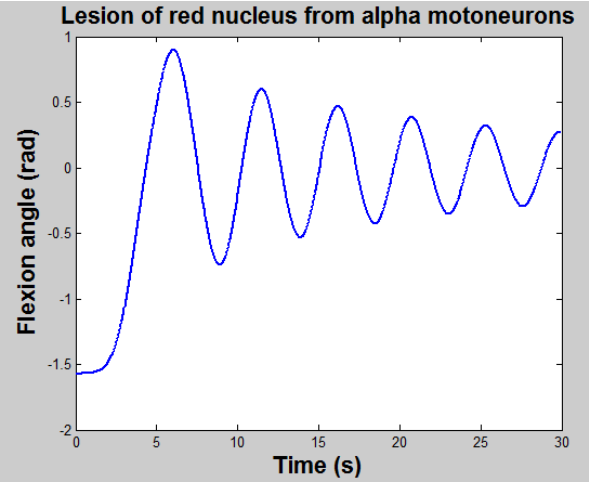

Figure 23: Oscillatory joint trajectory of an impaired model. Removing cerebellar control of alpha motoneurons, dis-inhibits their activity thus leading to instabilities in motion.

II. Cortical VITE model

The cortical VITE model, based on Equations 44 - 57, was also simulated separately. Parameters used in this model are shown below. Again, two versions of each sub-model were used to simulate interactions between agonist and antagonist motor pathways and muscle groups. Figure 24 displays the overall structure of the model that

includes the simplified models of extrafusal and intrafusal fibers. Figure 25 displays the internal structure of the update VITE model, with the agonist-antagonist feedback explicitly shown.

$\nu = 0.1;$	$B^{(u)} = 0.01;$	$h = 0.025;$	$I = 200;$
$\theta = 0.7;$	$B^{(r)} = 0.1;$	$\psi = 15;$	$V = 10;$
$\rho = 0.07$	$\eta = 0.7;$	$k = 1;$	
$\phi = 1;$	$\Theta = 0.7;$	$\tau = 5;$	
$G_0 = 0.75$	$\delta = 0.1;$	$\Lambda = 0.003;$	

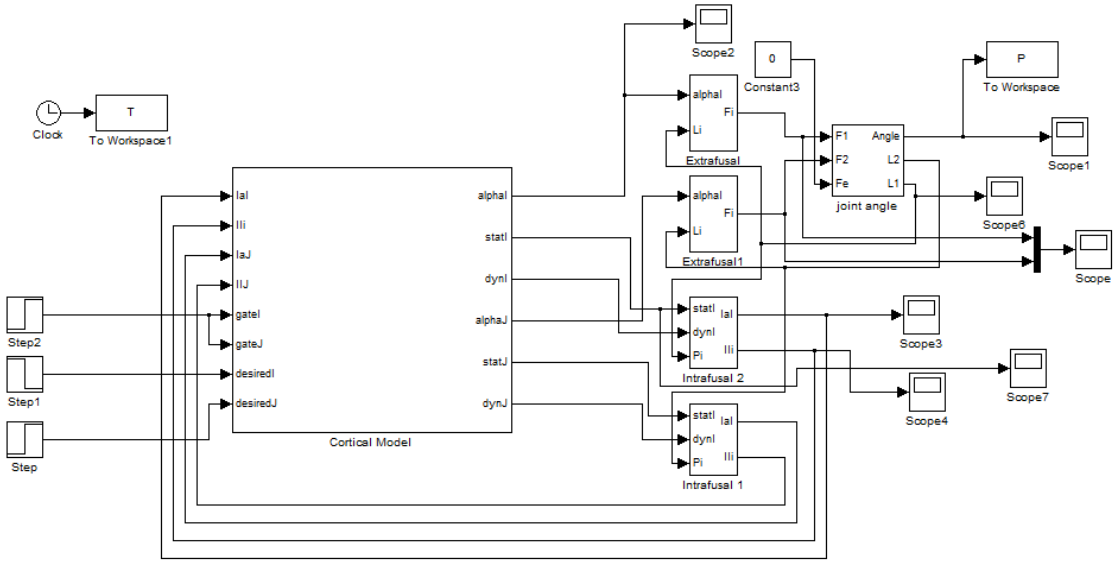

Figure 24: Cortical VITE simulink model. Although the VITE model is improved, the muscle fiber models and the spinal models are greatly simplified.

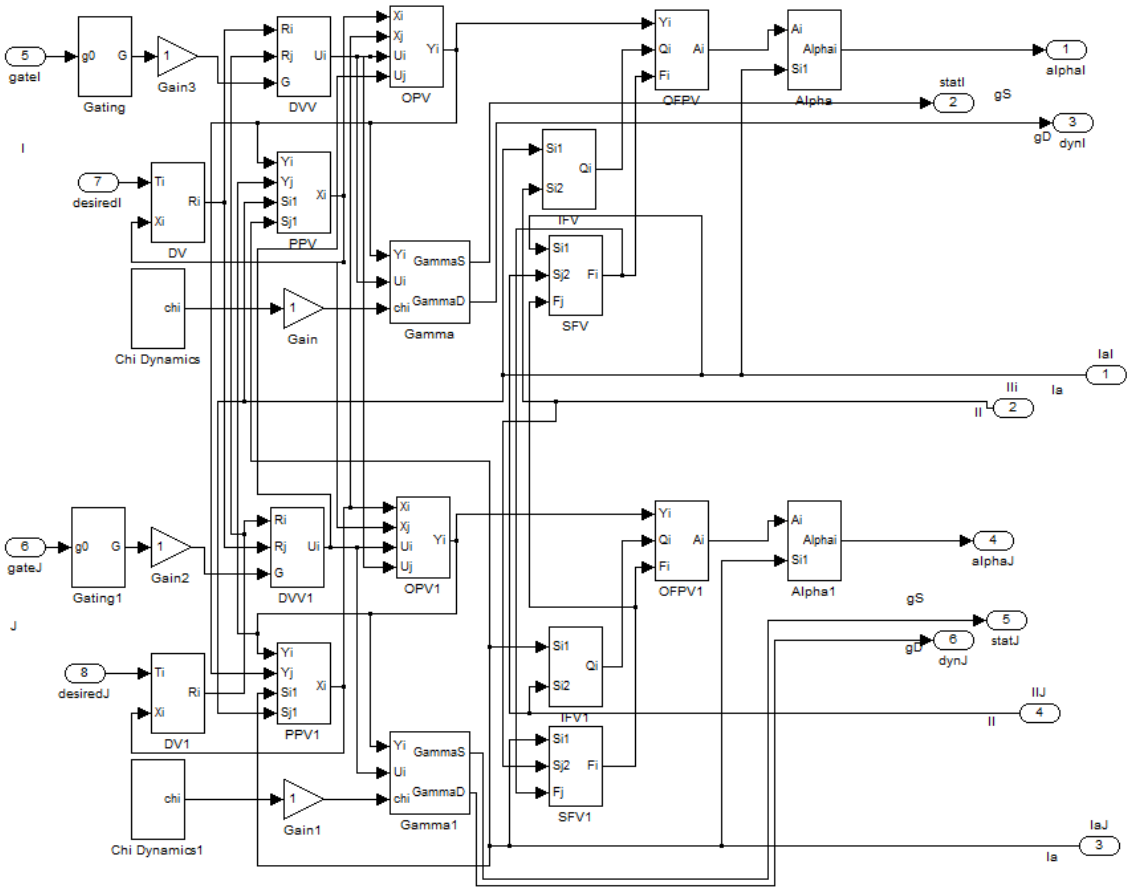

Figure 25: Detailed view of the VITE model. Note the large cross-connectivity between agonist and antagonist control streams. This coordinates activation of these muscle groups.

Despite using parameter values similar to those indicated by Cisek, Bullock, and Grossberg, the generated model did not accurately reproduce their results. Simplified extrafusal and intrafusal muscle fiber models may be the cause of the poor results produced by the cortical VITE model. However, the differentiation between tonic, phasic, and phase - tonic cells in M1, makes this model interesting from a physiological stand point. This model also takes into account the effect of the efference copy and the spindle afferent signals on the perceived position vector; something not seen in the original VITE model.

This model also required a long simulation time to complete, which indicates that the parameters were designed for a slower time scale. Parameter values can be scaled to simulate real-time motions.

III. Combined update VITE and FLETE-CBM model

It was hypothesized that to improve the performance of the VITE-FLETE-CBM model, the cortical VITE model can be included in the BSM model. The resultant model consisted of the updated difference vector (DV), perceived position vector (PPV), and outflow position vector (OPV) models, as well as the original CBM and FLETE models.The complete model structure is seen in Figure 26. Parameters were scaled so that all models were compatible. New parameter values are listed below; unlisted parameter values remained unchanged.

$G_o = 2.6;$ $B^{(r)} = 0.001;$ $n = 0.25;$

$C = 40;$ $\eta = 2.1;$ $\lambda = 8.5;$

$\epsilon = 1;$ $\Theta = 70;$ $P = 0.4;$

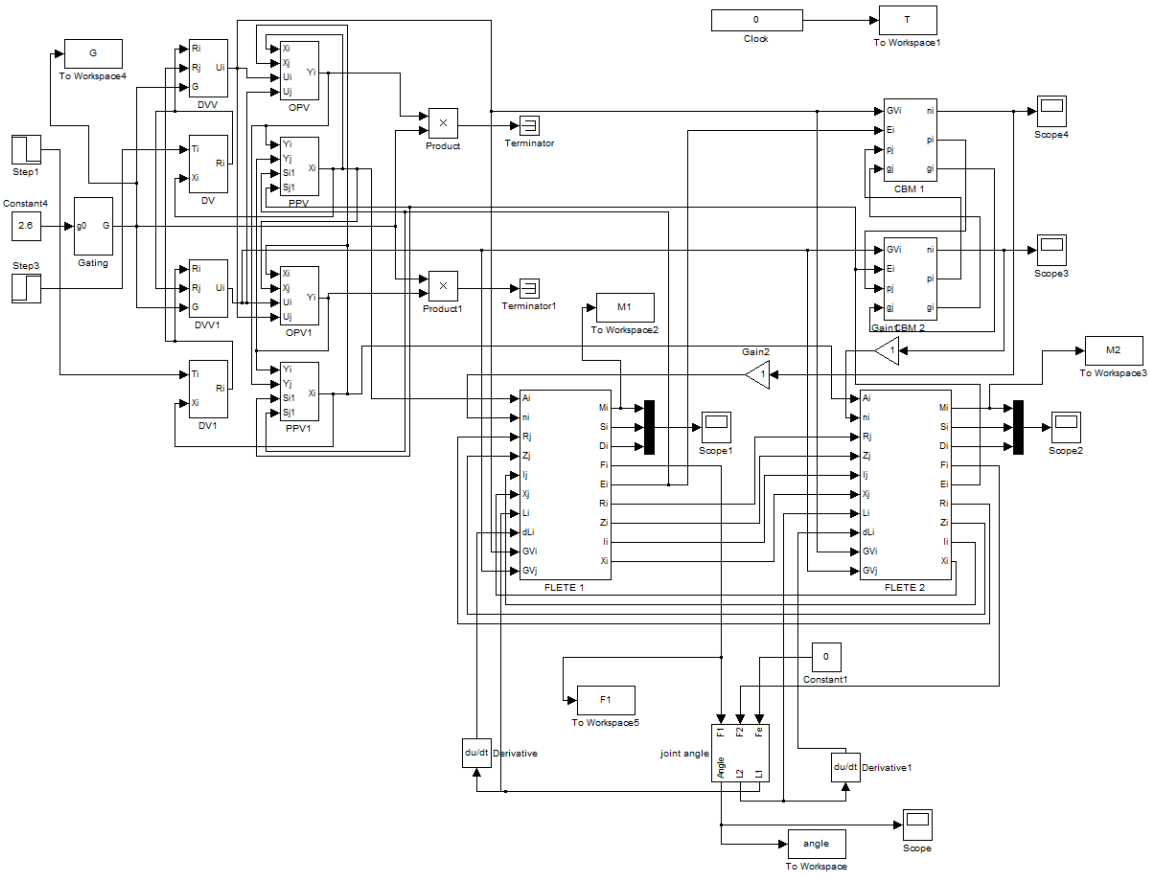

Figure 26: Combined model with the expanded VITE model with the FLETE and CBM models.

BSM provides insight into the physiological signals that control smooth motion.Figure 27 displays the intact joint trajectory simulated by the BSM model to two different targets, one near (left) and the other far (right). Again, there are overshoots, as well as slight oscillations at the end of motion that may or may not occur in human motion. These oscillations may be occurring because the FLETE model does not incorporate ligament dynamics, which would dampen the motion faster. Note that the overshoot and oscillations seen for the larger movement (right) is similar in amplitude to the left movement, but are scaled smaller.

Analysis was also performed on the alpha motoneuronsignals driving the antagonist muscle groups. Figure 28 shows the two alpha motoneuron signals. Although at the end of motion, these signals are balanced, which indicates a state of equal co-contraction, they do not return to rest, e.g. zero activation. This is another fault of the model; it is assumed that when rest state is reached, all signals return to zero.

Recorded single joint trajectories of normal subjects can be used to solve for the proper alpha motoneuron activities by inverting equations 14, 56, and 57. However, the inverse problem is underdetemined since both agonist and antagonist muscle forces and alpha motoneuron activities are unknown, while only the angular trajectory of the motion is known. An adaptive method, similar to that described by Ferrarin [16], to compute these unknowns. The adaptive system uses an inverted system to calculate the unknown variables, and then the forward system to recalculate the known input. The difference between the actual input to the inverse system and the output of forward system is used to adapt parameters within the inverse system. When the output of the forward system matched the known input, then a true inverse solution has been determined, and the unknown variables can be extracted. This method is beyond the scope of this thesis, therefore true alpha motoneuron activities were not calculated and it was hypothesized that by completing the unified BSM model, the proper physiological signals will be uncovered.

One possible cause for the improper alpha motoneuron signals, calculated by the Cortical VITE - FLETE - CBM model,may be the gating signal that initiates motion and ensures smooth start-up.As seen in Figure 29, the gating signal increases to the G_0 value is a sigmoid-like fashion, but then remains active throughout the motion. A realistic

gating signal should inactivate at the end of motion, and decrease close to the end of motion. Therefore, a more realistic basal ganglia gating model was explored.

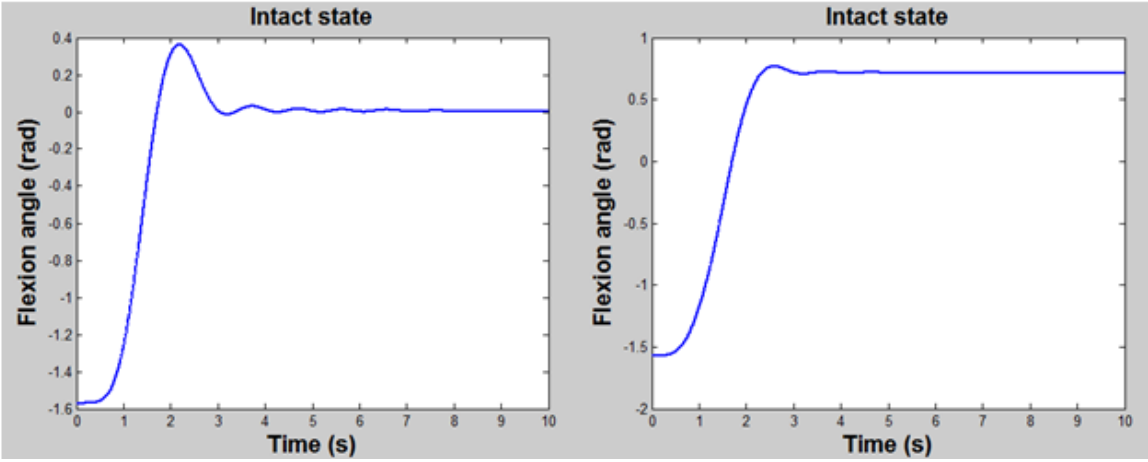

Figure 27: Two intact trajectories generated by the combined model. Note the reduced overshoot compared to the original VITE-FLETE-CBM model. Note scale difference

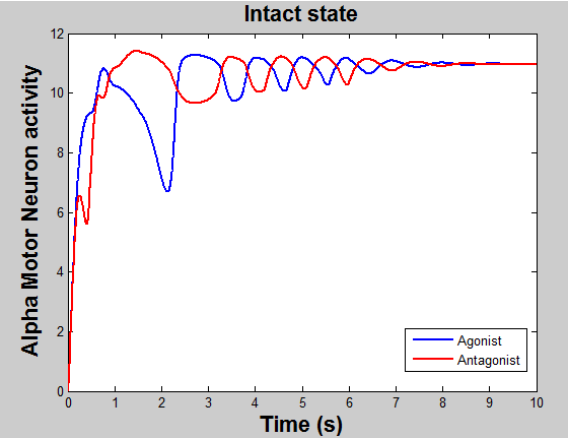

Figure 29: Agonist and antagonist alpha motoneuron signals. At the end of motion, these signals do not return to rest.

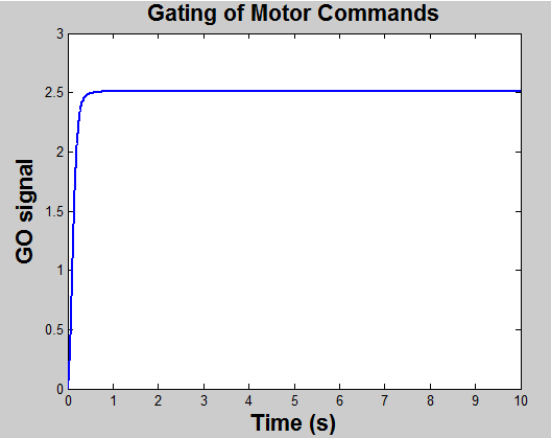

Figure 28: Simulated Go signal generated by basal ganglia. Again, at the end of motion, this signal does not return to zero.

IV. Contreras-Vidal & Stelmach (CVS) Basal Ganglia Model

The basic basal ganglia and thalamus model was developed using Equations 58 - 64.The output of the thalamus, *Pk*, acts as the gating signal in the VITE model. Figure 30 displays the thalamic signal based on the parameter values and inputs listed in the original study. Unlike the gating signal produced by the VITE model, this signal initiates as a sigmoid-like which then returns to zero after motion is complete, as expected. Thus the CVS model simulated a more realistic command. Similar thalamic signals were simulated in the original study; the rate of growth and decay of the gating signal modulates that velocity and duration of the produced motion.

Although, this simple basal ganglia model is sufficient to produce a more realistic thalamic gating signal, it is difficult to combine this model with models of other brain systems. More accurate and optimized basal ganglia models have since been developed, therefore this model is not utilized in the combined neuromuscular control model.

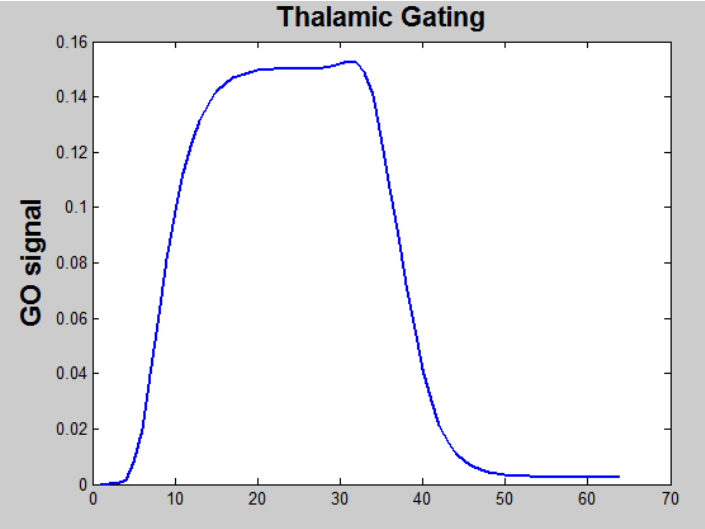

Figure 30: Thalamic gating signal generated by Contreras-Vidal's and Stelmach's model. At the end of motion, the Go signal returns to zero.

V. LIST PARSE

The combined VITE-FLETE-CBM model requires two inputs, the gating signal and a target position vector. The gating signal of Figure 30 is too simple to generate real motion; similarly, the assumed target position vector is also simplified. A step function target position vector was used as input to the model, initiating at the current limb position and stepping to the target limb position when the motion is intended to begin. It is difficult to assume that neurons can produce sharp, non-differentiable signals such as the step function. LIST PARSE attempts to simulate the generation of the target position vector, as well as working memory functionality.

A model of a two item ISR task was developed based on the equations provided by Pearson and Grossberg. Two targets were presented in series to the model and were encoded into working memory via one item list chunks. After a volitional signal was triggered, the system recalled the targets in order of appearance, and finally generated a target position vector for each target. A simple VITE model was also added to generate a

joint trajectory based on the target position vector. A six item ISR task was also simulated to evaluate the effect of larger item sets on the performance of the model.

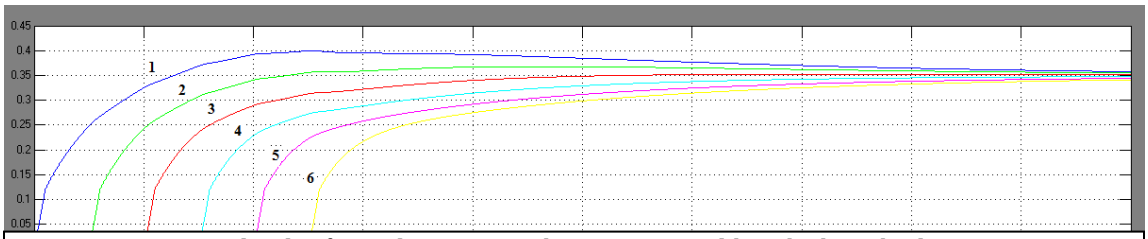

Figure 31: Activation levels of stored items in working memory. Although, their absolute activations may change, order of items is preserved.

Layers 4 and 6 are responsible for generating the activity gradient of stored items in working cognitive memory. Since both lists contain only2 or 6 items, the produced activity gradient should resemble a primacy gradient: first item has the highest activation, while the last item has the lowest activation. The result is seen in Figure 31, activation levels of the stored items reflects the order the items were presented. Volitional triggering by the basal ganglia initiates the rehearsal wave that signals for item recall. The volitional signal is set as a step function, and the motor gating signal, G, is calculated via a leaky integrator equation shown below (Eq 66):

$$\frac{dG}{dt} = -G + V_m \tag{66}$$

Again, just like in the VITE-FLETE-CBM model, the gating signal is too simplified, and does not resemble the form of the thalamic signal in Figure 30. Note, that the gating signal has no method for reset. Thus this model can only model one transition from working memory encoding to recall, but not vise-versa.

As described in the Literature Review section, once the target item is recalled and selected in the pre-SMA and dorsolateral PFC, the learned target is used to create a target position vector. The is seen in equation 67.

$$\frac{dT_i}{dt} = -0.5T_i + (1 - T_i) * (100(S_i - 0.5)^+) \tag{67}$$

Once the target is no longer selected (because the motion has completed, and a new target is needed), the target position vector self-inhibits to prevent reactivation of this motion. This feature is also not seen in the VITE-FLETE-CBM model where the target position vector always remains active. Resultant target position vectors for the two item simulation are seen in Figure 32.

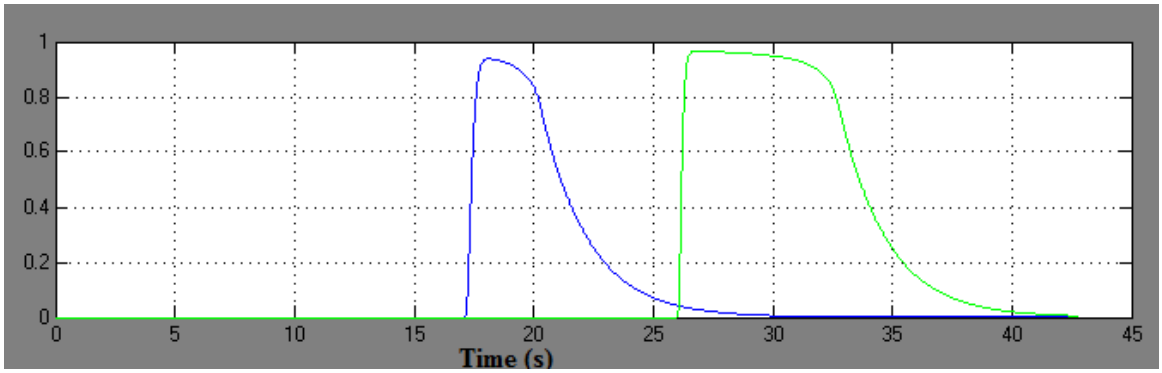

Figure 32: Target position vector signals generated by the LIST PARSE model. At the end of motion, these signals return to zero, unlike the step function signals used in the VITE-FLETE-CBM model.

The target position vectors, however, do not encode directionality of motion or the absolute location of the target. Further modifications of the model are required, to include that information in the generated signal, since they are required for the proper functioning of the VITE-FLETE-CBM model, as well as for normal human motion.

VI. lisTELOS modified

Eye saccade generation was simulated using the lisTELOS model provided by Dr. Silver [61]. lisTELOS, as described in the previous section, models multiple brain structures associated with eye saccade planning. Hypothetically, by slightly adjusting these brain system models, it would be possible to simulate visually guided limb motion planning.

Visual targets or series of targets would similarly excite the posterior parietal cortex, but instead of the LIP, the MIP would be responsible for representing the target and limb in eye-centered coordinates. Working memory function would remain in the PFC, thus this model would not change. For eye saccades, target selection occurs in the selection eye field, SEF, which is a specialized region of the pre-SMA. For limb motion, the same function would occur in the pre-SMA, however, the model would not change significantly. The frontal eye field, FEF, is responsible for generating a saccade plan; for limb motion, similar functions occur in the premotor cortex and the SMA. They should generate the proper target position vector that would then act as an input to the VITE-FLETE-CBM model. It is assumed that the FEF output plans, generated by this model, can be used to represent the target position vector. The premotor cortex would also coordinate the target and the limb to be reflected in the same reference frame (i.e, the target must be in the limb's reference frame).The same basal ganglia loops should remain for controlling the rehearsal wave and the competition of motion plans in the premotor cortex/SMA.

Many studies have shown that the superior colliculus helps control of eye saccades and head rotation, but its role in limb motion is unclear. Some studies have suggested that neurons deep in the superior colliculus may be important for hand-eye

coordination [64]. For limb motion, the primary motor cortex is analogous to the superior colliculus. Similarly, the primary motor cortex is gated by the basal ganglia. To modify the lisTELOS model, the superior colliculus sub-unit would be replaced by a VITE model, gated by the third basal ganglia loop.

The FEF model tracks the end of a saccade via post-saccadic inhibitory cells. These cells threshold the superior colliculus burst, and cause inhibition of the current selected saccade plan when the burst exceeds that threshold. This ensures that the plan will be fully removed, prior to selection of a new saccade plan, and right after the completion of the current saccade. This is not applicable for limb motion, since the superior colliculus does not participate in limb motion planning. Additionally, no evidence has been found for performance-rate-estimator cell mentioned in the LIST PARSE model. It is hypothesized that the difference vector (DV), generated in Brodmann area 5 can be used to track completion of motion. For point-to-point motion, the DV will always reach zero at the end of motion.

Using these assumptions, the lisTELOS model was combined with the simplified VITE model (Equations 10 and 11). Equations describing the original lisTELOS model [61] were altered to generate the target position vector (TPV), DV, and perceived position vector (PPV). Equations 68 - 70 can be used with the published lisTELOS model to generate these values.

$$\frac{dTPV_i}{dt} = (1 - TPV_i) * \left(80 * \left(\frac{FO_i^4}{0.5^4 + FO_i^4}\right) + 100 * \left(\frac{PL_i^4}{0.5^4 + PL_i^4}\right)\right) - TPV_i * (800 * [GN_i - 0.3]^+ + 10) \tag{68}$$

$$\frac{dDV_i}{dt} = TPV_i - DV_i - PPV_i \tag{69}$$

$$\frac{dPPV_i}{dt} = [DV_i]^+ * [0.3 - GN_i]^+ \quad (70)$$

In the lisTELOS model, FO_i and PL_i, represent the activity of the FEF and LIP, respectively. Based on the assumptions stated above, these values would now represent the activities of the SMA and MIP. The target position vector represents the release of motion plans by the premotor cortex when the SMA and MIP are coherent.

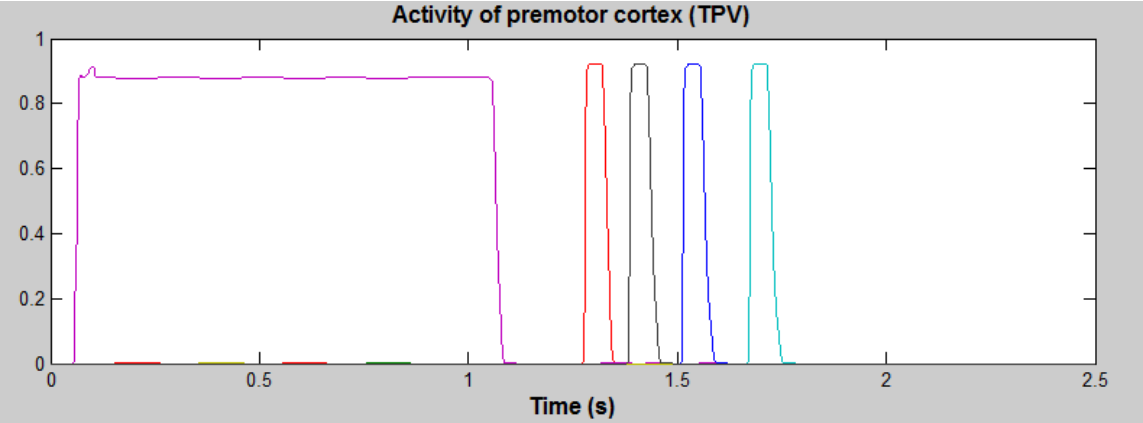

Figure 33: Target position vector signals generated for four consecutive targets. For the first second, the system remains at rest and is shown 4 targets in order. Next, the system recalls these targets from memory and produces TPVs for each discrete motion.

As seen in the TELOS, LIST PARSE, and lisTELOS models, targets and plans are spatially organized into parallel and competing channels. Channels represent the activity of parallel neuron clusters. Therefore, as seen in Figure 33, the desired movement target is represented by activation of a particular channel. Parallel encoding of movement target and release of movement plans (activation of TPV), must be decoded into a serial target position vector that reflect the current position and the desired end position. The serial TPV is used to drive the cortical VITE-FLETE-CBM model, discussed above. Similarly, the calculated DV and PPV signals seen in Figure 34are a representation of the movement trajectory to a desired target, but do not fully reveal the absolute movement of the limb in space.

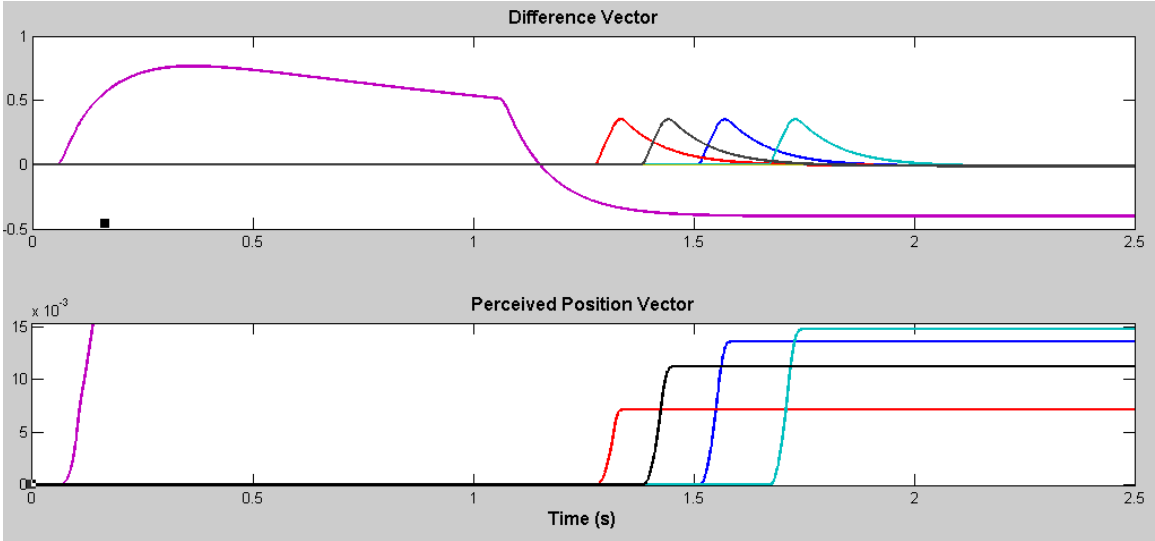

Figure 34: Top: Difference vector is used to determine the end of a motion and the recall of the next target. Bottom: Produced perceived position vectors. Note that the scale of these trajectories are not absolute. In both top and bottom: The purple trace is analogous to the superior colliculus burst due to the fixation point.

Additionally, the current equations generate an extraneous signal seen starting with in the first ten seconds of the simulation. In the original lisTELOS model, this signal represented a superior colliculus burst caused by the fixation point. In limb motion, the initial position should not generate a TPV since no movement is necessary. Further analysis is required to understand how the fixation point signal functions for limb motion. However, an initial attempt was made, where a new TPV signal, a scalar TPV signal, was generated to remove the effects of the fixation point. The scalar TPV signal multiplies the a serialized version of TPV by the movement distance, as seen in Figure 35. Thus, the fixation point signal would be eliminated since the movement distance is zero. It is hypothesized that this scalar TPV signal is then relayed by the primary motor cortex to the descending motor pathways to generate physical limb motion, while the parallelized

TPV, DV and PPV signals continue to be used within the brain structure to create an internal representation of the desired motion.

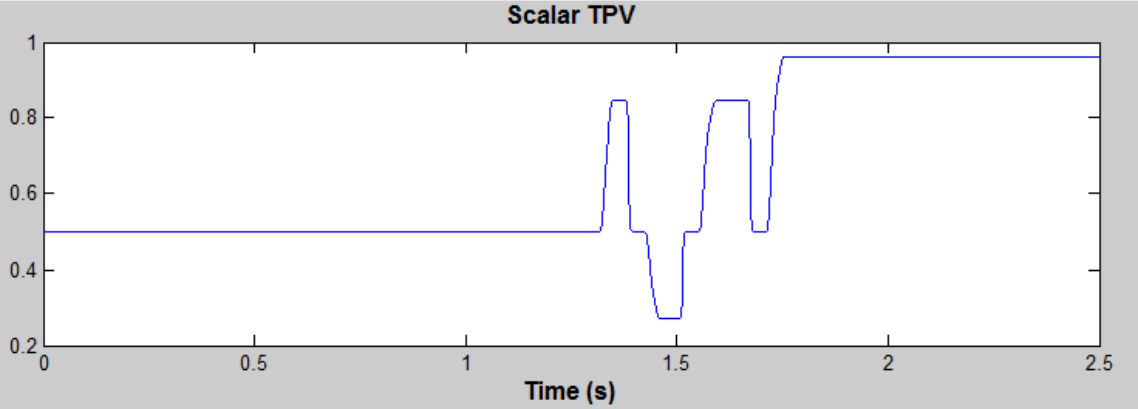

Figure 35: Scalar TPV represents the desired limb positions in space. Note that the fixation point TPV seen in figure 33 is no longer present since the movement distance is zero. Scalar TPV a serialized representation of TPV, representing both spatial and temporal information.

Finally, the current model does not explain how desired movement velocity in encoded. VITE-FLETE-CBM and the thalamocortical model assumed that the desired velocity is described by the magnitude of the GO function (thalamic gating signal) generated by the basal ganglia. However, the movement plan gating signal, GN_i, in the lisTELOS model does not describe velocity. It is used only to trigger the release of movement plans from the premotor cortex, as seen by the term $[0.3\text{-}GN_i]^+$.This suggests that a separate basal ganglia pathway may be responsible for controlling the desired velocity, or vigor, of motion. Studies have indicated that dopamine dependent cortico-striatal pathways modulate motor output and thus the rate of movement [65]. Such a pathway may be approximated by the basal ganglia model proposed by Contreras-Vidal and Stelmach. Further analysis needs to be done to combine the modified lisTELOS model with the basal ganglia - thalamocortical model.

These initial assumptions and modifications of existing models facilitate the unification of voluntary motor control models and involuntary motor control models; yet certain questions still exist. Hypotheses #2 and #3 remain unproven until further neurophysiological and computational studies are performed to determine the full relationship between all areas involved with motor control.

Conclusions:

The brain - spinal cord - muscle model (BSM), attempts to simulate full neuromuscular control of single joint motion ranging from the generation of a motion plan to the contraction of muscle groups to move the limb. No previous model has attempted to include so many elements of physiological control to explain how human motion is planned, executed, monitored, and adapted in unison. Detailed models of voluntary single joint limb motion were produced by integrating several published models of the brain and the neuromuscular system. Modeling neuromuscular control of motion requires the incorporation of both of muscle and brain physiology. Many isolated models of a particular aspect of the neuromuscular system have been developed, but they have not been integrated into a comprehensive neuromuscular control. Here, some of the most advanced and physiologically relevant models are presented, are selectively combined into a more complete model.

An extrafusal muscle model developed by Riener and Quintern was incorporated into the single joint model by Ferrarin et al. where the generated isometric force was modulated via the muscles' force-length and force-velocity properties and was further influenced by joint elasticity and viscosity. This model successfully produced flexion around the knee joint when muscles were externally stimulated by a PWM

pattern.Attempts to use the FLETE model to drive Ferrarin's joint model proved unsuccessful, therefore FLETE's slightly simplified extrafusal muscle model was used instead. Although the PWM pattern is meant to emulate alpha motoneuron activity, it was difficult to relate this signal to alpha motoneuron signal generated by the FLETE model.

An intrafusal muscle model was presented by Mileusnic et al. and Dan Song that differentiated between nuclear bag fibers and nuclear chain fibers. Dang Song's Virtual Arm model incorporated in intrafusal fiber model along with a virtual muscle model, SIMM, and a Golgi tendon organ model. This model remained open-loop since it required input of alpha and gamma motoneuron activations in order to generate movement. FLETE contained a fairly detailed intrafusal fiber model that differentiated between dynamic fibers (bag_1 fibers) and static fibers (bag_2 and chain fibers). These fibers were innervated by dynamic and static gamma motoneurons, respectively, and returned Ia, II, and Ib afferent signals.

The cortico-spinal tract and the rubro-spinal tract, and their interaction with the cerebellum, was incorporated into the FLETE model. Spinal tracts execute motor commands generated by the primary motor cortex, and coordinate activation of antagonist muscle groups. This coordination control is performed by spinal interneurons, specifically Renshaw cells. These cells prevent over stimulation of alpha motoneurons to prevent muscle injury by tetanus. They also co-activate antagonist alpha motoneurons to stabilize movement and prevent tremor. A similar function is carried out by the cerebellum; although unlike Renshaw cells which are passive, the cerebellum learns proper timing control between antagonist muscle groups. The cerebellum also fine tunes motion by comparing ascending sensory information to motor commands delivered

through the nucleus interpositus cells and the red nucleus. This provides a fast response mechanism since sensory information is accessed prior to its integration in the somatosensory cortex.FLETE models the cerebellum as an adaptive neural network that represents the function of the associated cell types.

The primary motor cortex is modeled by VITE. This model takes the movement plans and converts them to movement commands. Movement plans are encoded in the target position vector, which contain information about the distance and direction of the target from the current limb position. Movement commands are realized by the perceived position vector before they get sent to the spinal tracts. The PPV creates an internal representation of the desired limb trajectory, which will be further modulated by motion errors relayed by muscle afferents. Cisek, Bullock, and Grossberg created a detailed VITE model that accounts for phasic, tonic, and phase-tonic cells in the primary motor cortex.

Generation of motion plans is not as well understood as the execution of them. Planning requires contributions from many brain systems, specifically the basal ganglia, prefrontal cortex, parietal cortex, premotor and supplementary motor cortices, and the somatosensory cortex, as well as others. Grossberg and others have developed a computational method, Adaptive Resonance Theory, to explain how plans are generated and how decisions about these plans can be made by these brain systems. It was noted that out of all of brain systems, the basal ganglia is most prominently responsible for gating the output of various brain structures and is the site of competition between motor plans.

Several models have been developed applying ART to eye saccades and item learning. lisTELOS is the most advanced eye saccade model that incorporates storage and recall of multiple targets to/from working memory, selection of saccade targets by the SEF, generation of saccade plans by the FEF, competition of these plans in the basal ganglia, and the execution of these plans by the superior colliculus. It was hypothesized that the eye saccade planning mechanism is similar to limb motion planning. Many of the brain structures involved in eye saccades, have analogous brain structure involved with limb motion. Although, their anatomical locations may it is hypothesized that analogous brain system have largely similar functions and thus can be modeled in the same way. Therefore, the planning pathway for limb motion would involve the prefrontal cortex for storage and recall of motion targets, the pre-SMA for selection of motion targets, the SMA and premotor cortex for generation of motion plans, the basal ganglia for competition of these plans, and the primary motor cortex for execution of chosen plans. Additionally, the posterior parietal cortex is involved to represent motion targets in eye-centered, head-centered, and limb-centered reference frames, and to aid with the function of the primary motor cortex.

Herein, brain systems, spinal pathways, and muscle functions were examined in detailed models. Multiple published models were analyzed and combined to increase their analytical power. New insights into certain brain disorders could be seen from simulations. Although, it is not yet possible to combine all the models, future work can be done to improve compatibility between them. This study provides a detailed framework of the pieces required to build a physiologically relevant neuromuscular model. The uses

of such a model would include analysis of impaired motion and the creation of a human-like robotic actuator.

Bibliography:

1. Beard, S., A. Hunn, and J. Wight. "Treatments for Spasticity and Pain in Multiple Sclerosis: A Systematic Review." *Health Technology Assessment* 7.140 (2003): 1-111. Print.
2. Mehrholz, Jan, Katja Wagner, Daniel Meissner, Kay Grundmann, Christian Zange, Rainer Koch, and Marcus Pohl. "Reliability of the Modified Tardieu Scale and the Modified Ashworth Scale in Adult Patients with severe Brain Injury: A Comparison Study."*Clinical Rehabilitation* 19.7 (2005): 751-59. Print.
3. Syczewska, Malgorzata, Maria K. Lebiedowska, and Anand D. Pandyan. "Quantifying Repeatability of the Wartenberg Pendulum Test Parameters in Children with Spasticity." *Journal of Neuroscience Methods* 178.2 (2009): 340-44. Print.
4. Widmaier, Eric P., Hershel Raff, and Kevin T. Strang. *Vander's Human Physiology: The Mechanisms of Body Function.* 11th ed. Boston: McGraw-Hill, 2008. Print.
5. Riener, R., and J. Quintern. "A Physiologically Based Model of Muscle Activation Verified by Electrical Stimulation." Bioelectrochemistry and Bioenergetics 43.2 (1997): 257-64. Print.
6. Zajac, Felix E. "Muscle and Tendon: Properties, Models, Scaling, and Application to Biomechanics and Motor Control." *Critical Reviews in Biomedical Engineering*17.4 (1989): 359-410. Print.
7. Mileusnic, M. P. "Mathematical Models of Proprioceptors. I. Control and Transduction in the Muscle Spindle." *Journal of Neurophysiology* 96.4 (2006): 1772-788. Print.
8. Paxinos, George, and Jürgen K. Mai. "Peripheral Nervous System and Spinal Cord." *The Human Nervous System*. San Diego, CA: Academic, 2004. 118. Print.
9. Mileusnic, M. P. "Mathematical Models of Proprioceptors. II. Structure and Function of the Golgi Tendon Organ." *Journal of Neurophysiology* 96.4 (2006): 1789-802. Print.
10. Song, Dan. *Model - Based Studies of Control Strategies for Noisy, Redundant Musculoskeletal Systems*. Diss. University of Southern California, 2008. Print.
11. Song, D., N. Lan, G. E. Loeb, and J. Gordon. "Model-Based Sensorimotor Integration for Multi-Joint Control: Development of a Virtual Arm Model." *Annals of Biomedical Engineering* 36.6 (2008): 1033-048. Print.
12. Maltenfort, M. G. "Spindle Model Responsive to Mixed Fusimotor Inputs and Testable Predictions of Beta Feedback Effects." *Journal of Neurophysiology* 89.5 (2003): 2797-809. Print.
13. Manuel, Marin, and Daniel Zytnicki. "Alpha, Beta and Gamma Motoneurons: Functional Diversity in the Motor System's Final Pathway." *Journal of Integrative Neuroscience* 11.3 (2011): 243-76. Print.
14. Eldrich, Thomas, Robert Riener, and Jochen Quintern. "Analysis of Passive Elastic Joint Moments in Paraplegics." *IEEE Transactions on Biomedical Engineering* 47.8 (2000): 1058-065. Print.
15. Riener, Robert, and Thomas Edrich. "Identification of Passive Elastic Joint Moments in the Lower Extremities." *Journal of Biomechanics* 32.5 (1999): 539-44. Print.
16. Ferrarin, Maurizio, Francesco Palazzo, Robert Riener, and Jochen Quintern. "Model-Based Control of FES-Induced Single Joint Movements." *IEEE Transactions On Neural Systems and Rehabilitation Engineering* 9.3 (2001): 245-56. Print.

17. Riener, Robert, and Thomas Fuhr. "Patient-Driven Control of FES-Supported Standing Up: A Simulation Study." *IEEE Transactions On Rehabilitation Engineering* 6.2 (1998): 113-24. Print.
18. Wininger, Michael. "A Regressed Phase Analysis for Coupled Joint Systems." *Gait & Posture* 33.1 (2011): 136-39. Print
19. Valero-Cuevas, Francisco J., Heiko Hoffmann, Manish U. Kurse, Jason J. Kutch, and Evangelos A. Theodorou. "Computational Models for Neuromuscular Function."*IEEE Reviews in Biomedical Engineering* 2 (2009): 110-35. Print.
20. Fisher, Karen M., Demetris S. Soteropoulous, and Claire L. Witham. "The Motor Cortex and Descending Control of Movement." *Advances in Clinical Neuroscience and Rehabilitation* 11.6 (2012): 11-13. Print.
21. Lemon, Roger N. "Descending Pathways in Motor Control." *Annual Review of Neuroscience* 31.1 (2008): 195-218. Print.
22. "DESCENDING MOTOR PATHWAYS." *DESCENDING MOTOR PATHWAYS*. CNS Clinic Jordan, n.d. Web. 22 Dec. 2013. <http://neurophysiology.ws/desendingmotorpathways.htm>.
23. Contreras-Vidal, J. L., S. Grossberg, and D. Bullock. "A Neural Model of Cerebellar Learning for Arm Movement Control: Cortico-spino-cerebellar Dynamics." *Learning & Memory* 3.6 (1997): 475-502. Print.
24. Bullock, Daniel, Raoul M. Bongers, MarnixLankhorst, and Peter J. Beek. "A Vector-integration-to-endpoint Model for Performance of Viapoint Movements." *Neural Networks* 12.1 (1999): 1-29. Print.
25. Van Der Smagt, Patrick. "Cerebellar Control of Robot Arms." *Connection Science* 10.3-4 (1998): 301-20. Print.
26. Ramnani, Narender. "The Primate Cortico-cerebellar System: Anatomy and Function."*Nature Reviews Neuroscience* 7.7 (2006): 511-22. Print.
27. Fritschy, Jean-Marc, Dr. *Anatomy of the Cerebellum*. Zurich: Zentrum Für Neurowissenschaften Zürich, 5 Nov. 2012. PDF.
28. Ngyuen - Vu, T D Barbara. "Cerebellar Purkinje Cell Activity Drives Motor Learning."*Nature Neuroscience* 16.12 (2013): 1734-739. Print.
29. Najafi, Farzaneh, and Javier F. Medina. "Beyond "all-or-nothing" Climbing Fibers: Graded Representation of Teaching Signals in Purkinje Cells." *Frontiers in Neural Circuits*7.115 (2013): 1-7. Print.
30. Seeberger, Lauren C. *Cerebellar Tremor – Definition and Treatment*. Rep. Colorado Neurological Institute, 2005.Web. 28 Apr. 2013. <http://www.thecni.org/reviews/17-fall05-p31-seeberger.pdf>.
31. Wolpert, Daniel M., Chris R. Miall, and MitsuoKawato. "Internal Models in the Cerebellum."*Trends in Cognitive Sciences* 2.9 (1998): 338-47. Print.
32. Cisek, Paul, Stephen Grossberg, and Daniel Bullock. "A Cortico-Spinal Model of Reaching and Proprioception under Multiple Task Constraints." *Journal of Cognitive Neuroscience* 10.4 (1998): 425-44. Print.
33. Krakauer, J., &Ghez, C.Voluntary movement. In E. R. Kandel, J. H. Schwartz, & T. M. Jessell (Eds.), *Principles of neural science*. 4th ed., pp. 756–781. New York: McGraw Hill, 1999. Print.
34. Kalaska, John F., Dan A. D Cohen, Martha L. Hyde, and Michel Prud'homme. "A Comparison of Movement Direction-Related Versus Load Direction-Related Activity

in Primate Motor Cortex, Using a Two- Dimensional Reaching Task." *The Journal of Neuroscience* 9.6 (1989): 2080-102. Print.
35. Mulero-Martinez, Juan I. "Neuromuscular-Like Control for an Artificial Finger with SMA Actuators." *AI 2006: Advances in Artificial Intelligence*. By Francisco Garcia-Cordova. Vol. 4304. N.p.: Springer Berlin Heidelberg, 2006. 678-88. Print. Lecture Notes in Computer Science.
36. Eliasmith, Chris, Terrence C. Stewart, Xuan Choo, Trevor Bekolay, Travis DeWolf, Yichuan Tang, and Daniel Rasmussen. "A Large-Scale Model of the Functioning Brain."*Science* 338 (2012): 1202-205. Print.
37. Redgrave, Peter. "Basal Ganglia." *Scholarpedia*. Web. 25 Dec. 2013. <http://dx.doi.org/10.4249/scholarpedia.1825>.
38. Miller, Earl K., and Jonathan D. Cohen. "An Integrative Theory of Prefrontal Cortex Function." *Annual Review of Neuroscience* 24 (2001): 167-202. Print.
39. Coutlee, Christopher G., and Scott A. Huettel. "The Functional Neuroanatomy of Decision Making: Prefrontal Control of Thought and Action." *Brain Research* 1428 (2012): 3-12. Print.
40. Hoffstaedter, Felix, Christian Grefkes, Karl Zilles, and Simon B. Eickhoff. "The "What" and "When" of Self-Initiated Movements." *Cerebral Cortex* 23.3 (2013): 520-30. Print.
41. Premji, Azra, Navjot Rai, and Aimee Nelson. "Area 5 Influences Excitability within the Primary Motor Cortex in Humans." *PLOS One* 6.5 (2011): 1-8. Print.
42. Bremner, Lindsay R., and Richard A. Andersen. "Coding of the Reach Vector in Parietal Area 5d." *Neuron* 75 (2012): 342-51. Print.
43. Cavanna, A. E. "The Precuneus: A Review of Its Functional Anatomy and Behavioural Correlates." *Brain* 129.3 (2006): 564-83. Print.
44. Colby, C., and J. Duhamel. "Spatial Representations for Action in Parietal Cortex." *Cognitive Brain Research* 5.1-2 (1996): 105-15. Print.
45. Grefkes, C., A. Ritzl, K. Zilles, and G. Fink. "Human Medial Intraparietal Cortex SubservesVisuomotor Coordinate Transformation." *NeuroImage* 23.4 (2004): 1494-506. Print.
46. Pesaran, Bijan, Matthew J. Nelson, and Richard A. Andersen. "Dorsal Premotor Neurons Encode the Relative Position of the Hand, Eye, and Goal during Reach Planning".*Neuron* 51.1 (2006): 125-34. Print.
47. Haruno, Masahiko, Gowrishankar Ganesh, Etienne Burdet, and MitsuoKawato. "Differential Neural Correlates of Reciprocal Activation and Cocontraction Control in Dorsal and Ventral Premotor Cortices." *Journal of Neurophysiology* 107 (2012): 126-33. Print.
48. Debaere, Filiep, Nicole Wenderoth, Stefan Sunaert, Paul Van Hecke, and Stephan P. Swinnen. "Internal vs External Generation of Movements: Differential Neural Pathways Involved in Bimanual Coordination Performed in the Presence or Absence of Augmented Visual Feedback." *NeuroImage* 19.3 (2003): 764-76. Print.
49. Nachev, Parashkev, Christopher Kennard, and Masud Husain. "Functional Role of the Supplementary and Pre-supplementary Motor Areas." *Nature Reviews Neuroscience* 9.11 (2008): 856-69. Print.

50. Contreras-Vidal, Jose Luis, and George E. Stelmach. "A Neural Model of Basal Ganglia-thalamocortical Relations in Normal and Parkinsonian Movement." *Biological Cybernetics* 73.5 (1995): 467-76. Print.
51. Turner, Robert S., Scott T. Grafton, John R. Votaw, Mahlon R. Delong, and John M. Hoffman. "Motor Subcircuits Mediating the Control of Movement Velocity: A PET Study." *Journal of Neurophysiology* 80.4 (1998): 2162-176. Print.
52. Contreras-Vidal, Jose L. "Computer Modeling in Basal Ganglia Disorders." *Atypical Parkinsonian Disorders*. Totowa, NJ: Humana, 2004. 95-108. Print.
53. Reed, Michael C., Frederik H. Nijhout, and Janet Best. "Computational Studies of the Role of Serotonin in the Basal Ganglia." *Frontiers in Integrative Neuroscience* 7.41 (2013): 1-8. Print.
54. Grossberg, Stephen. "Adaptive Resonance Theory: How a Brain Learns to Consciously Attend, Learn, and Recognize a Changing World." *Neural Networks* 37 (2013): 1-47. Print.
55. Kumar, Naveen. "Adaptive Resonance Theory." *Adaptive Resonance Theory*. 01 Dec. 2012. Web. 15 Dec. 2013. <http://www.slideshare.net/NaveenKumar11/adaptive-resonance-theory-15441260>.
56. Upal, Muhammad A., and Eric Neufeld. "Comparison of Bayesian and Neural Net Unsupervised Classification Techniques." MS.
57. Sekiai, Takaaki, Naohiro Kusumi, Yoshinari Hori, Satoru Shimizu, and Masayuki Fukai. "Auto Tuning Algorithm for Vigilance Parameter in the Adaptive Resonance Theory Model and Its Application to Fault Diagnosis System of Thermal Power Plants."*ASME 2011 Power Conference* 2 (2011). Print.
58. Brown, J. "How Laminar Frontal Cortex and Basal Ganglia Circuits Interact to Control Planned and Reactive Saccades." *Neural Networks* 17.4 (2004): 471-510. Print.
59. Grossberg, Stephen, and Lance R. Pearson. "Laminar Cortical Dynamics of Cognitive and Motor Working Memory, Sequence Learning and Performance: Toward a Unified Theory of How the Cerebral Cortex Works." *Psychological Review* 115.3 (2008): 677-732. Print.
60. Grossberg, Stephen. "Recurrent Neural Networks." *Scholarpedia*. 21 Feb. 2013. Web. 29 Dec. 2013. <http://www.scholarpedia.org/article/Recurrent_neural_networks>.
61. Silver, Matthew R., Stephen Grossberg, Daniel Bullock, Mark H. Histed, and Earl K. Miller. "A Neural Model of Sequential Movement Planning and Control of Eye Movements: Item-Order-Rank Working Memory and Saccade Selection by the Supplementary Eye Fields." *Neural Networks* (2011). Print.
62. Carpenter, R. H. S., and M. L. L. Williams. "Neural Computation of Log Likelihood in Control of Saccadic Eye Movements." *Nature* 377.6544 (1995): 59-62. Print.
63. Brodersen, Kay H., Will D. Penny, Lee M. Harrison, Jean Daunizeau, Christian C. Ruff, Emrah Duzel, Karl J. Friston, and Klaas E. Stephan. "Integrated Bayesian Models of Learning and Decision Making for Saccadic Eye Movements." *Neural Networks*21.9 (2008): 1247-260. Print.
64. Kleiser, Raimund, Veit Stuphorn, Lee E. Miller, and Klaus-Peter Hoffmann. "A Possible Role of the Superior Colliculus in Eye-hand Coordination." *Progress in Brain Research.* Vol. 134. Amsterdam: Elsevier., 2001. 109-25. Print.

65. Yin, H. H. "Action, Time and the Basal Ganglia." *Philosophical Transactions of the Royal Society B: Biological Sciences* 369.1637 (2014): 20120473. Print